NMR STUDY OF MAGNETIC SUPERCONDUCTOR

$RERh_4B_4$ (RE = Rare Earth)

Yoh Kohori

February 1984

Contents

ABSTRUCT

Pulsed NMR study has been performed in $RERh_4B_4$ (RE = rare earth) to understand the magnetic and superconducting property of the compound microscopically.

The nuclear spin lattice relaxation time T_1 of ^{89}Y, ^{103}Rh and ^{11}B have been measured in non-magnetic YRh_4B_4 and $LuRh_4B_4$ in order to investigate the density of states at each atomic site in $RERh_4B_4$. The observed T_1^{-1}'s are compared with the value that are obtained by using the calculated density of states for $RERh_4B_4$. The agreement of the experimental results with the band calculation is satisfactory for Y(RE) and Rh site. Considerable reduction of the density of states at RE site has been observed. This reduction is responsible for the weak coupling of RE spin and the superconducting electron at Rh_4B_4 cluster.

In $RERh_4B_4$ with RE of magnetic ion, Knight shift of ^{11}B has been measured. The isotropic Knight shift is proportional to $(g_J-1)J$ for all $RERh_4B_4$. This means that the conduction electron spin polarization induced by unit RE spin is nearly the same for all $RERh_4B_4$.

The isotropic Knight shift of ^{103}Rh was measured in $SmRh_4B_4$. From the shift data, the conduction electron spin polarization at Rh site is estimated The obtained value is by one order of magnitude larger than that in Chevrel phase compound.

From T_1 of ^{11}B in $RERh_4B_4$, the s-f and/or d-f exchange interaction at RE site have been obtained from the Korringa spin fluctuation of RE spin. The obtained values are by one order of magnitude larger than those found in Chevrel phase compound. This means that s-f exchange interaction play an important role in $RERh_4B_4$ than in Chevrel phase compound.

The crystal field effect on RE ion has been obtained from T_1. For Dy based compound, the first excited state of J_z is 130 K above the ground state. This energy spacing is much larger than the exchange interaction between RE ions, then the magnetic properties are much affected by the crystal field effect.

In non-magnetic superconductor $LuRh_4B_4$, the superconducting energy gap at B site was obtained from T_1 of ^{11}B. The ratio of the energy gap to the superconducting critical temperature was found to be that of a weak coupling superconductor: $2\Delta(0)/k_B T_c = 3.5$.

In antiferromagnetic superconductor $SmRh_4B_4$, T_1 was measured both in the normal antiferromagnetic state (2.9 kOe) and in the superconducting antiferromagnetic state (790 Oe). Below 0.3 K, T_1 is proportional to T^{-1} in the normal state. This means the Weger mechanism governs T_1 of ^{11}B at low temperature. The nuclear Zeeman energy of ^{11}B relaxes to the conduction electron band at Sm site. There is no difference between T_1 in the normal state and the superconducting state above 790 Oe. This means Sm site is in gapless or nealy gapless state in this magnetic field.

We observed the zero field NMR of ^{11}B in $Dy(Ir_{0.7}Rh_{0.3})_4B_4$ and $Ho(Ir_{0.7}Rh_{0.3})_4B_4$. In Dy-based compound, we found the occurrence of the long range antiferromagnetic ordering above the superconducting transition temperature. The magnetic structure in Dy-based compound is considered to be the same as in Ho-based compound.

§1 Introduction

In recent years, several ternary compound systems have been discovered which contain large amounts of magnetic ions at regular lattice sites.[1] Among the ternary compound systems, the crystal structure of two rare-earth ternary compounds, $REMo_6(S,Se)_8$ and $RERh_4B_4$ attract much interest.[2,3] The superconductivity and the long range magnetic order often occur simultaneously in these compounds. As for $RERh_4B_4$, the superconductivity appears for RE = Y, Lu, Sm, Nd, Er and Tm.[3] In Er based compound the superconductivity occurs at high temperature and is destroyed by the long range ferromagnetic order at low temperature.[3] In Sm, Nd and Tm based compound, however, superconductivity occurs at high temperature and coexists with antiferromagnetic long range order at low temperature.[3] In these compounds the superconducting transition temperature is higher than the magnetic transition temperature. The magnetic structure of Er, Nd and Tm based compound are determined by neutron diffraction measurement.[3,4] Gd, Tb, Dy and Ho based compounds exhibit only ferromagnetic order and superconductivity does not appear.[3] The coexistence of antiferromagnetic order and superconductivity is also proposed in $Dy(Ir_xRh_{1-x})_4B_4$ and $Ho(Ir_xRh_{1-x})_4B_4$, with $0.5 < x < 0.8$.[5,6] In these compounds, the magnetic ordering temperature is higher than the superconducting transition temperature. The magnetic structure of Ho based compound is confirmed[7] while that of Dy based compound is not yet understood.

In these compounds the superconductivity is considered to be carried by Rh_4B_4 cluster, while the magnetism is carried by RE atoms. The exchange interaction between RE magnetic moment and the conduction electron is considered to be small. Jarlborg et al. have carried out the band calculation and obtained the density of states at each atomic site.[8] The density

of states at RE site is responsible for the coupling of RE spin and the superconducting electrons, while that at Rh site is responsible for the condensation energy of the superconductivity. Jarlbolg et al. attributed the relatively small density of states at RE site to the coexistence of magnetic order and superconductivity. It is necessary to investigate the result of band calculation experimentally. It is also important to know the magnitude of exchange interaction between 4f-electron of RE ion and the conduction electron, which yields the exchange field on the super-conducting electron.

The $RERh_4B_4$ compounds exhibit comlex magnetic properties. For example, Dy compound has the highest T_m in the series of simple ferromagnetic compound from Gd to Ho.[3] Shenoy interpleted this phenomenon by taking account the crystal field effect, assuming that the RKKY interaction is proportional to RE spin.[9] It is necessary to confirm this assumption and also to estimate the magnitude of the conduction electron spin polarization for the understanding of the magnetic properties of $RERh_4B_4$.

Furthermore it is important to study the interplay of the super-conductivity and the magnetism in coexistent state. The antiferromagnetic order coexists with the superconductivity in $RERh_4B_4$. The temperature dependence of upper critical field implies the reduction of pair breaking effect in the antiferromagnetic state. We intend to study how the super-conducting energy gap is modified in antiferromagnetic superconductor. As s-f exchange scattering occurs at RE site, the energy gap may be much affected in RE site than in Rh site. It is therefore important to investigate the energy gap at each atomic site.

In this paper, NMR studies are performed to understand the above problem from the microscopic point of view. We intend to study the reason why the superconductivity and the magnetic order coexist in this compound.

Next we intend to know how the superconducting and magnetic property are modified in antiferromagnetic superconductor.

In order to study the coupling of RE moment and the superconducting electrons at Rh_4B_4 cluster, we will investigate the density of states at each atomic site, the conduction electron spin polarization at Rh and B site and also the s-f and/or d-f exchange interaction between RE and the conduction electrons.

The density of states at each atomic site is evaluated from the nuclear spin lattice relaxation time T_1 of respective nuclei. T_1 is determined by the square of both hyperfine field and density of state. From T_1 one can estimate the density of states at each site. Thus we shall measure T_1 of ^{89}Y, ^{103}Rh and ^{11}B in non-magnetic compounds YRh_4B_4 and $LuRh_4B_4$.

The exchange field on the superconducting electron and also the RE dependence of the magnitude of RKKY interaction are obtained from the conduction electron spin polarization, which yields an isotropic Knight shift in non-magnetic nuclear species in the paramagnetic state. We shall measure the Knight shift of ^{103}Rh and ^{11}B in $RERh_4B_4$ and obtain information about the conduction electron spin polarization at Rh and B site.

The s-f and/or d-f exchange interaction between the 4f-electron of RE and the conduction electron yields the Korringa spin fluctuation of RE moment. The Korringa spin fluctuation of RE spin enhances T_1^{-1} of ^{11}B through the magnetic dipole coupling and RKKY coupling between RE and ^{11}B. Thus T_1 of ^{11}B provies informations about s-f exchange interaction at RE site.

The crystal field effect affects the RE spin fluctuation. Then we obtain an information about the crystal field effect from the analysis of T_1.

In order to determine the superconducting energy gap in antiferromagnetic superconductor, we shall measure T_1 of ^{11}B in $SmRh_4B_4$ in antiferromagnetic and superconducting state. When T_1 is governed by the relaxation to the conduction electrons, T_1 is proportional to T^{-1} in the normal state and increases exponentially in superconducting state owing to the appearance of the superconducting energy gap in the conduction electron band. Hence from the measurement of T_1, one can confirm the appearance of superconductivity and obtain the magnitude of energy gap. Furthermore by the measurement on respective nuclei, we can determine the energy gap at each atomic site.

It is necessary to confirm the antiferromagnetic order of $Dy(Ir_xRh_{1-x})_4B_4$ and make similar investigation as in $SmRh_4B_4$, since more informations are expected to be available in Dy compound as the coexistence region in Dy compound is larger than in $SmRh_4B_4$.

§ 2 Experimental procedures

1) Sample preparations

The samples of $RERh_4B_4$ were prepared by arc melting in an argon atmosphere. The starting elements were rare earth of 99.9% purity, Rh of 99.95% purity and B of 99.8% purity. Weight loss after melting was typically 1% in these compounds. The ingots were annealed at $1100°C$ for 7 days in a tantalum crucible under high vacuum. The ingot was crushed to powder (about 74 μm) for the NMR and X-ray measurements. X-ray analysis showed that the sample formed the $CeCo_4B_4$ structure.[10]

2) T_c measurements

The superconducting transition temperature was measured by susceptibility measurement (Shawlow Devline method).[11]

3) ^{4}He cryostat and ^{4}He flow cryostat

Temperature between 1.2K and 4.2K was obtained by pumping liquid ^{4}He. The temperature was determined by vapor pressure. Temperature above 4.2 K was achieved by passing helium gas over the sample. The temperature was determined by a thermo-couple junction placed near the sample.

4) ^{3}He cryostat

A cryostat used for NMR study at ^{3}He temperature is of the single-cycle type. Figure 1. illustrates the apparatus. ^{3}He pot is made of Pb glass which does not contain B. As B in usual soda glass sometimes prevented our B NMR study, we used Pb glass for ^{3}He pot.

Incoming ^{3}He gas is liquified through a tube which is in thermal

contact with a ^{4}He bath(1.45 K), and liquid ^{3}He enters ^{3}He pot. Finally

the ^{3}He pot becomes filled with liquid and a temperature 0.45 K is achieved

by pumping. The temperature was measured by carbon resistor in liquid ^{3}He.

The resistor was calibrated against the NMR intensity and T_1 of Pt.($T_1 T$

= 29.2 msec for Pt which is used in this measurement) The temperature

was controiled by feedback of the thermometer output to the heater in

liquid ^{3}He. A superconducting magnet was immersed in liquid ^{4}He to provide

steady magnetic field. Receiver coil was wound on a sample to maximize filling

factor and was immersed directly in liquid ^{3}He. The transmitter coil was

located in ^{4}He bath to avoid the rf heating.

^{3}He PUMPING
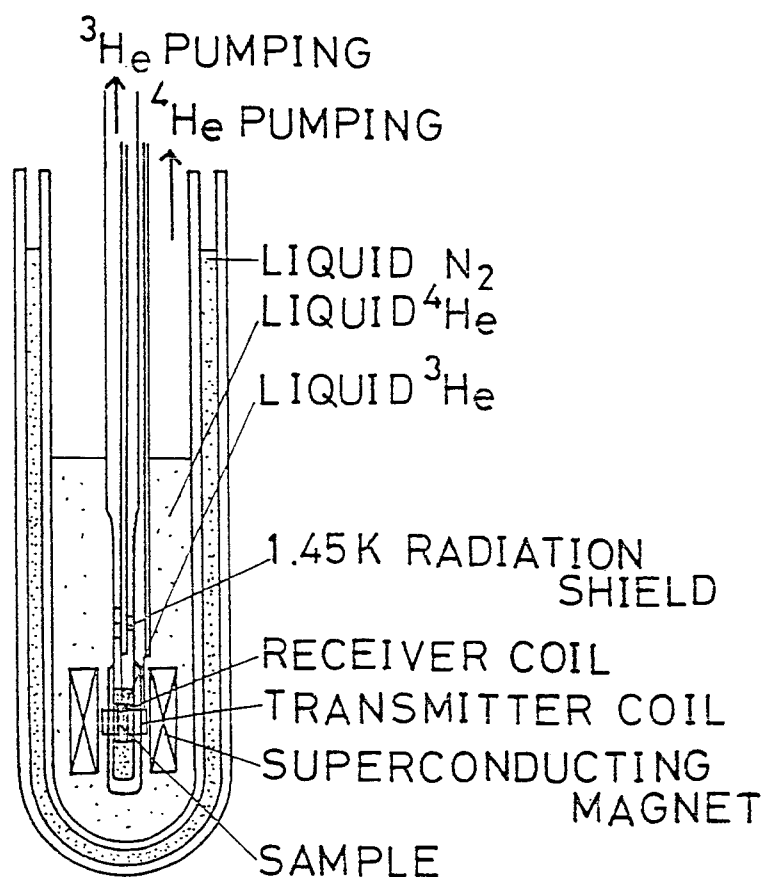
^{4}He PUMPING

LIQUID N$_2$
LIQUID ^{4}He

LIQUID ^{3}He

1.45 K RADIATION
            SHIELD
RECEIVER COIL
TRANSMITTER COIL
SUPERCONDUCTING
            MAGNET
SAMPLE

Fig.1 The single-cycle type ^{3}He cryostat and the NMR arrangement

5) Dilution refrigerator

^{3}He-^{4}He dilution refrigerator has been used to obtain low temperature below 0.3 K The principal parts of a continuously operating dilution refrigerator are shown in Fig. 2-1. The phase separation occurs in the mixing chamber and cooling is produced there by driving ^{3}He atoms from the boundary to the lower dilute phase. The continuous dissolution of ^{3}He atoms from the concentrated to the dilute phase is obtained by circulating ^{3}He in the system by means of a pump at room temperature. Incoming gas is first precooled and liquified in the condenser attached to the ^{4}He pot (1.1K). The liquid then enters the still at o.7K, the continuous exchanger, the step heat exchangers and finally the mixing chamber. After crossing the phase boundary, ^{3}He atoms driven by an osmic pressure gradient, proceed through the heat exchangers to the still and are removed from the still by pumping. A commercial Oxford Instrument 150 microwatt dilution refrigerator was used for this investigation. The base temperature of this dilution refrigerator is 11.0 mK and cooling power at 100 mK is 150 microwatt. The experimental arrangement is shown in Fig. 2-2. The sample was in direct contact with liquid helium inside the mixing chamber. In order to produce cooling at the base of the long glass tube, it is necessary to bring the concentrated helium 3 stream close to the powdered sample. To do this a bent stainless steel tube is provided. The sample temperature was measured by carbon resistance thermometer at the mixing chamber. The resistor was calibrated against the NMR intensity and T_1 of Pt .

The crossed coil system was used for NMR. The cylindrical receiver coil of 0.01 mm diameter was wound on the glass tube to maximize the filling factor and was thermally anchored to the mixing chamber. The transmitter coil was saddle shape and was thermally anchored to the cold plate. The steady magnetic field was produced by a Helmholz coil, which was located in the ^{4}He bath. Warming up of the sample by eddy current was excluded by reduced repititon rate. The base temperature was 40 mK with applying rf pulses.
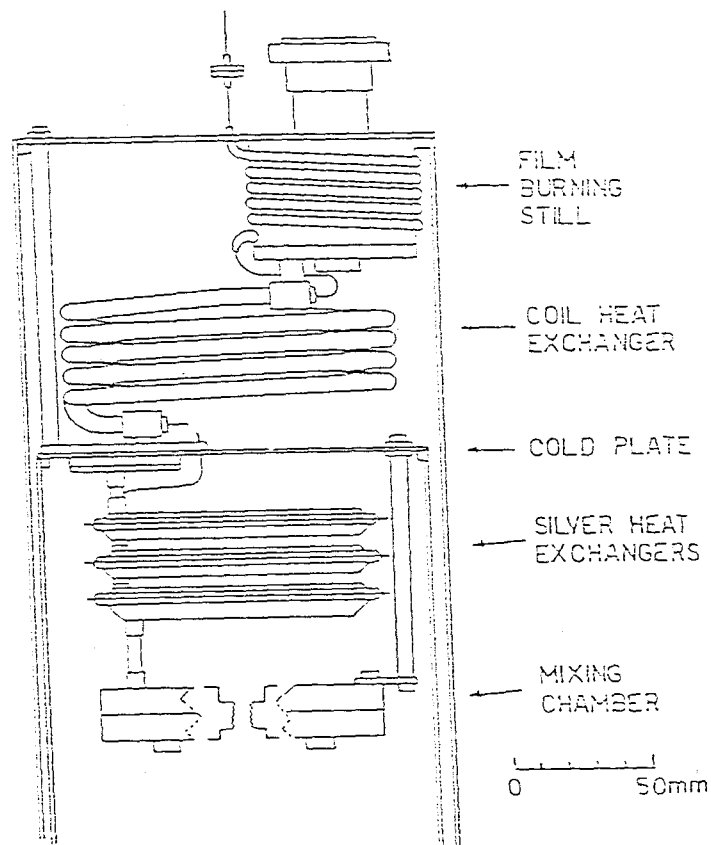
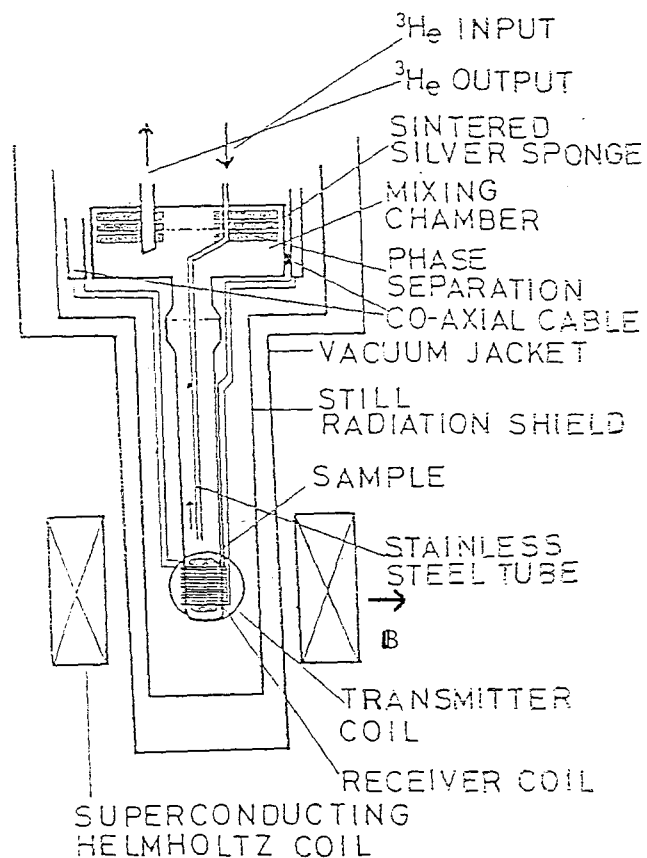Fig.2-1   The principal parts of a continuously operating dilution refrigerator

Fig.2-2   The NMR arrangement in the dilution refrigerator

6) NMR technique

The NMR shift, line width and spin lattice relaxation time T_1 are important paramaters in metal , being sensitive probes of the character of the conduction electron spins at the Fermi surface and character of the localized moments.

The NMR measurements were performed by the phase coherent pulsed spectrometer in the frequency range of 1-20 MHz. In the measurement of low frequency NMR, the signal averager was used to improve the signal to noise ratio. Furthermore, the fast recovery of the receiver system was secured with a shunt chopper .

6-1) Resonance shift measurement

Resonance shift of ^{11}B and ^{103}Rh were obtained by the following frequency field ratio. [12)]

^{11}B: ν/H = 1.366 KHz/Oe , ^{103}Rh: ν/H = 0.13 KHz/Oe

6-2) T_1 measurement

In many systems encountered in NMR, when the interactions contributing to the line width (quadrupolar or magnetic) are so strong that ΔH_{inhomo} is much larger than H_1 , the spin system can not be saturated completely by the single pulse. Then the recovery of the nuclear spin after the single pulse is not exponential which yields an ambiguity in T_1 measurement. The problem of incomplete spin saturation can frequently be circumvented by using the saturation comb method. The saturation comb consists of a train of n identical (n= 4-20) , equally spaced pulses applied within a time less than T_1. This pulse train is followed by a pulse-echo sequence to monitor the recovered magnetization. Indeed we have used a train of 10 saturation pulses above 1.2 K, and about 80% of nuclear magnetization recovers exponentially. In the temperature below 1K, rf heating becomes a serious problem, and special precautions(e.g., reduced pulse repetition rate , reduced number of saturation pulses.) were necessary to assure reliable data. At ^{3}He temperature , pulse repetition rate is 5-10 sec and number of saturation pulses is 3-5 . When

we used ^{3}He-^{4}He dilution refrigerator, pulse repetition rate is 20-30 sec

and number of saturation pulses is 2-3.

About 40% of the nuclear magnetization recovers exponentially in this .

pulse condition.

§3 The crystal structure of $RERh_4B_4$

The structure of ternary rhodium borides was determined by Vandenberg and Mattias [10] as shown in Fig. 3. The lattice parameters of the Rh compounds are shown in Table 1. The space group is $P4_2/nmc$ (No. 137), with the atomic position as follows (origin at $\overline{4}m2$) 2RE in 2(b) (0,0,1/2), (1/2,1/2,0); 8Rh in 8(g) $(0,x_{Rh},z_{Rh})$, etc., with $x_{Rh}=0.248$, $z_{Rh}=0.137$: 8B in 8(g): $(x_B, 0,z_B)$, etc., with $x_B = 0.325$ and $z_B = 0.847$. The B atoms form pairs parallel to the a axis and are surrounded by five Rh atoms. The interatomic distance in the $CeCo_4B_4$ structure is shown in Table 2.

Table 1. Cell parameter of the tetragonal $RERh_4B_4$.

	a (Å)	c (Å)
YRh_4B_4	5.308	7.403
$NdRh_4B_4$	5.333	7.468
$SmRh_4B_4$	5.312	7.430
$GdRh_4B_4$	5.309	7.417
$TbRh_4B_4$	5.303	7.404
$DyRh_4B_4$	5.302	7.395
$HoRh_4B_4$	5.293	7.379
$ErRh_4B_4$	5.292	7.374
$TmRh_4B_4$	5.287	7.359
$LuRh_4B_4$	5.294	7.359

Table 2 Interatomic distance in YRh_4B_4 (in Å)

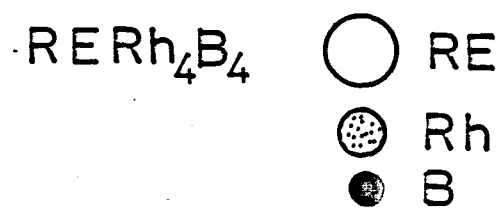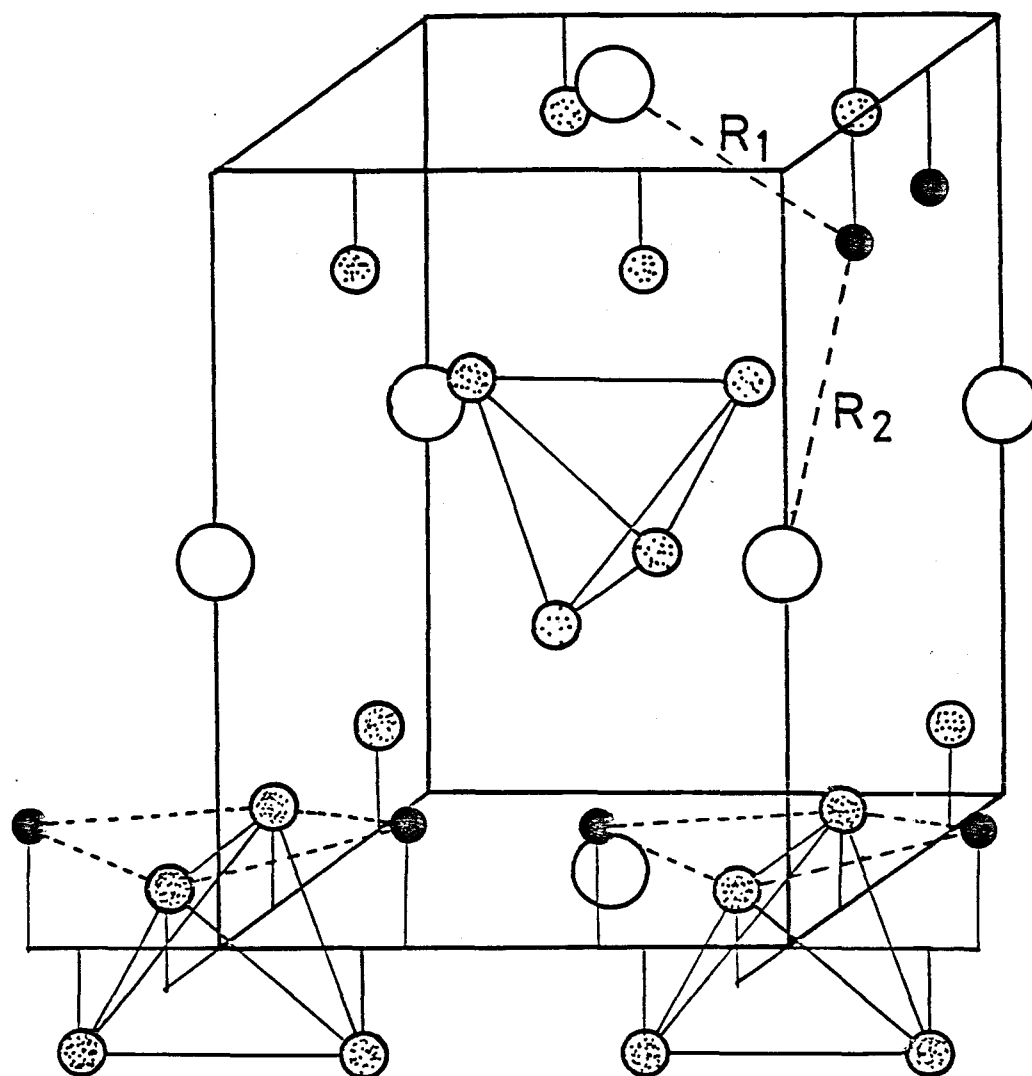| Rh-1Rh: 2.63	Y -4Rh: 2.99	B -2Y : 3.03
-2Rh: 2.75	-8Rh: 3.14	-1Y : 3.09
-1Rh: 2.66	B -1RH: 2.17	
-2Rh: 3.14	-2Rh: 2.17	
B -1B : 1.86	-2Rh: 2.25	

$RERh_4B_4$ RE
               Rh
               B

Fig.3 The crystal structure of $RERh_4B_4$

§4 Experimental results and discussions

(1) Non-magnetic compounds YRh_4B_4 and $LuRh_4B_4$

The highest superconducting temperatures among the $RERh_4B_4$ compounds are displayed by the non-magnetic compounds $LuRh_4B_4$ (T_s = 11.5K), which has a completely filled 4f electron shell and YRh_4B_4 (T_s = 10.8K) which has no 4f electrons.[3] We performed NMR study of YRh_4B_4 and $LuRh_4B_4$ to know the density of states at each site of $RERh_4B_4$ and the superconducting properties.

(1-1) The density of states (DOS) at RE, Rh and B site

In ternary boride $RERh_4B_4$ Jarlborg and Freeman carried out ab initio self-consistent band structure calculations on three of these ternary borides (Y, Ho and Er).[8] They have found that the weak f-s and f-d interaction in this compound is attributed to the negligibly small density of states of s-and p-electrons at RE site and small density of states of d-electron at RE site (1/3 the value of $N_d(E_F)$ in Ho metal) as shown in Table 3.

In order to investigate DOS at each site experimentally, we measured the nuclear spin lattice relaxation time of ^{89}Y(RE site), ^{103}Rh and ^{11}B in YRh_4B_4 and $LuRh_4B_4$.   In the normal state , the relation T_1T = const. is observed for each site, which is shown in Fig.4 and Fig.5, respectively. T_1T of ^{103}Rh in YRh_4B_4 and $LuRh_4B_4$ are 25 secK, and T_1T of ^{89}Y is 92 secK. T_1T of ^{11}B is 55secK. T_1 of ^{11}B is also measured by Kumagai and Fradin,[13] their value is T_1T = 46 secK, which is slightly shorter than ours.

The important contributions to the relaxation rates arise from core-polarization hyperfine interaction with d-electron and orbital hyperfine interaction with p- and d- electron, as well as from the contact hyperfine interaction with s-electron. ($T_1T)^{-1}$ may be expressed as

$$R = R_s + R_{orb}^p + R_{cp}^d + R_{orb}^d \quad , \tag{1}$$

where R_s, R_{cp} and R_{orb} represent the rate through the Fermi contact, core-polarization and orbital hyperfine interactions, respectively. We simply estimate R_{cp} and R_{orb} in tight-binding approximation. Then R_s, R_{cp} and R_{orb} are written as following,

$$R_s = 2hk_B\gamma_N^2 \left(H_s \ N_s(E_F) \right)^2 \quad , \tag{2}$$

$$R_{orb}^p = 4hk_B\gamma_N^2 \left(H_{orb}^p \ N_p(E_F) \right)^2 \quad , \tag{3}$$

$$R_{orb}^d = 2hk_B\gamma_N^2 \left(H_{orb}^d \ N_d(E_F) \right)^2 \ (\ 2/3 \cdot f \cdot (2 - 5/3 \cdot f)) \quad , \tag{4}$$

$$R_{cp}^d = 2hk_B\gamma_N^2 \left(H_{cp}^d \ N_d(E_F) \right)^2 \ (\ 1/3 \cdot f^2 + 1/2 \cdot (1-f)^2) \quad , \tag{5}$$

where γ_N is the gyromagnetic ratio of the concerned nucleus. The density of states at the Fermi energy for s-, p- and d-electrons for one direction of the spin are denoted by $N_s(E_F)$, $N_p(E_F)$ and $N_d(E_F)$ respectively and f is the average fractional admixture of 4-d (Γ_5) state at the Fermi surface. We assume f=1 or 3/5 as R is not so sensitive to f. We refer the value H_s, H_{orb}^p and H_{cp}^d for ^{89}Y and ^{103}Rh to those of the pure Y and Rh metal following Asada et al.[14,15] These assumed values are given in Table 3 together with the calculated relaxation rate. This estimation agrees with the experimental relaxation rate. As for ^{11}B, we calculate T_1 by using the atomic hyperfine field H_s[16] and $N_s(E_F)$[8] at B site. The result is shown in Table 3. The calculated value is smaller than the experimental value. The discrepancy may become small if we take into account the contribution from p-electron and the change of the hyperfine field in the compound from the atomic value.
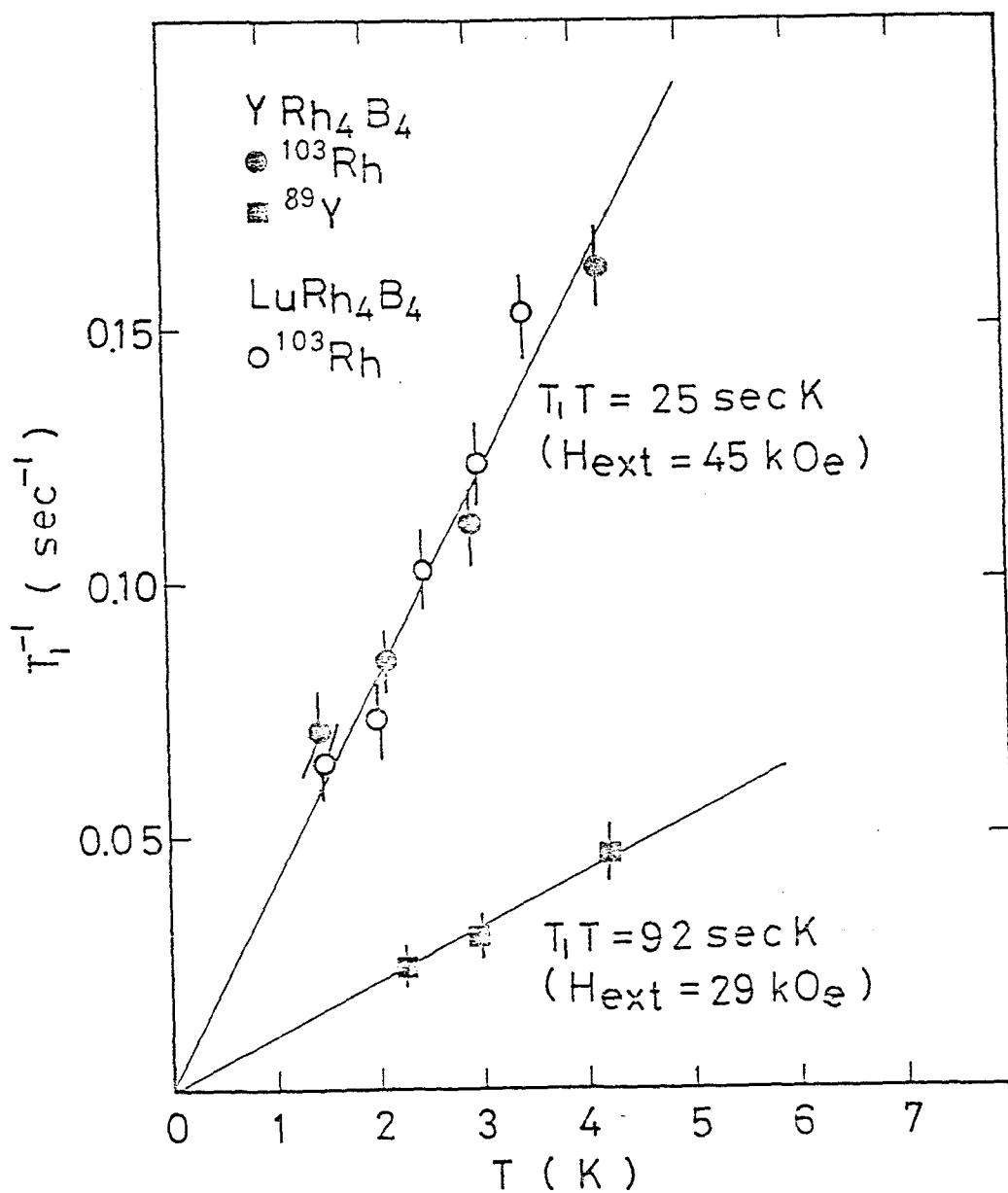
Fig.4　Temperature dependence　of T_1 of ^{89}Y and ^{103}Rh in YRh_4B_4 and $LuRh_4B_4$.
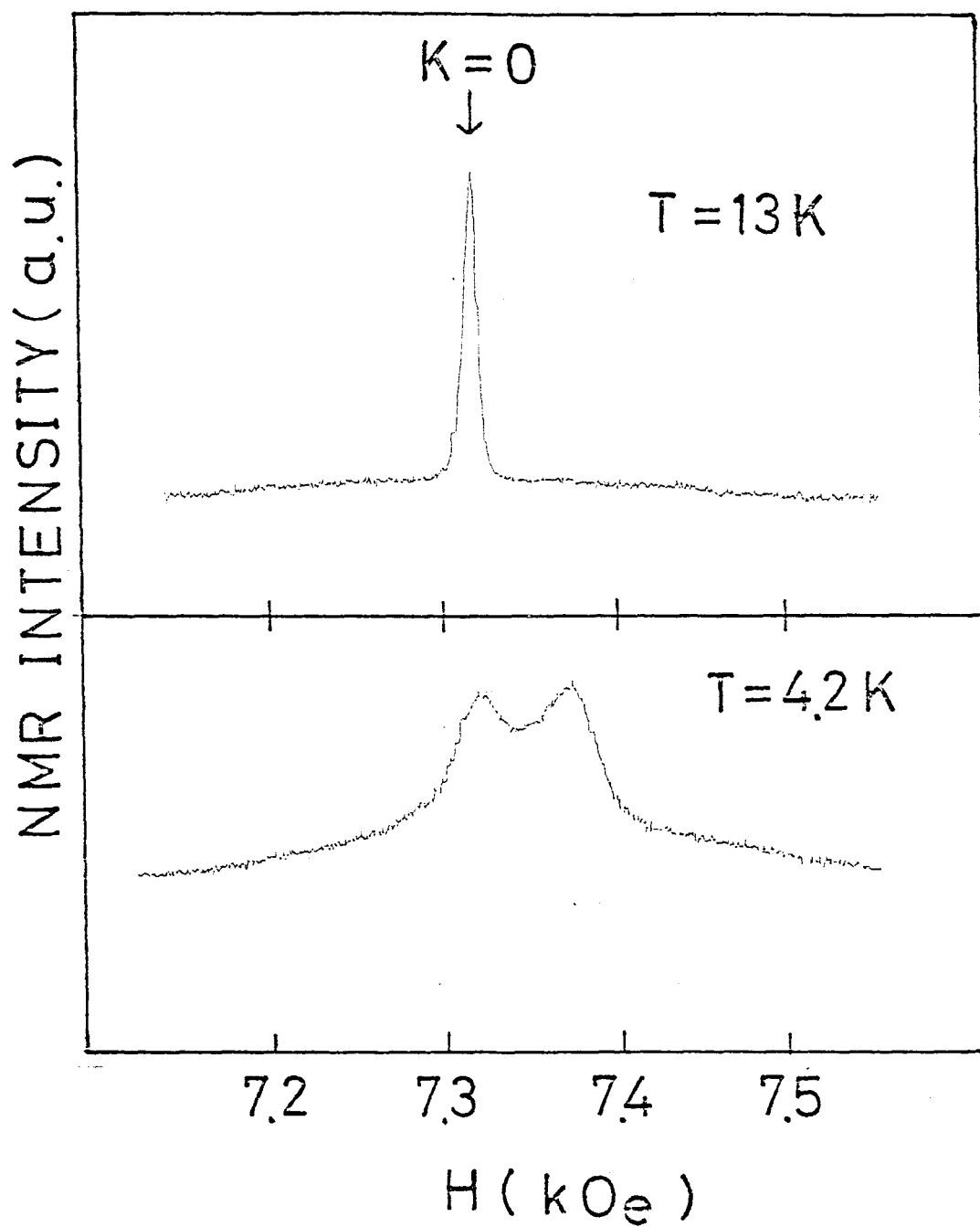
Fig. 5-1 ^{11}B NMR of ±1/2 transition of quadrupole split lines in $LuRh_4B_4$

The system is in normal state at T = 13 K.

Fig. 5-2 ^{11}B NMR spectrum in $LuRh_4B_4$ in superconducting mixed state. An

additional broadening and a negative shift are observed.

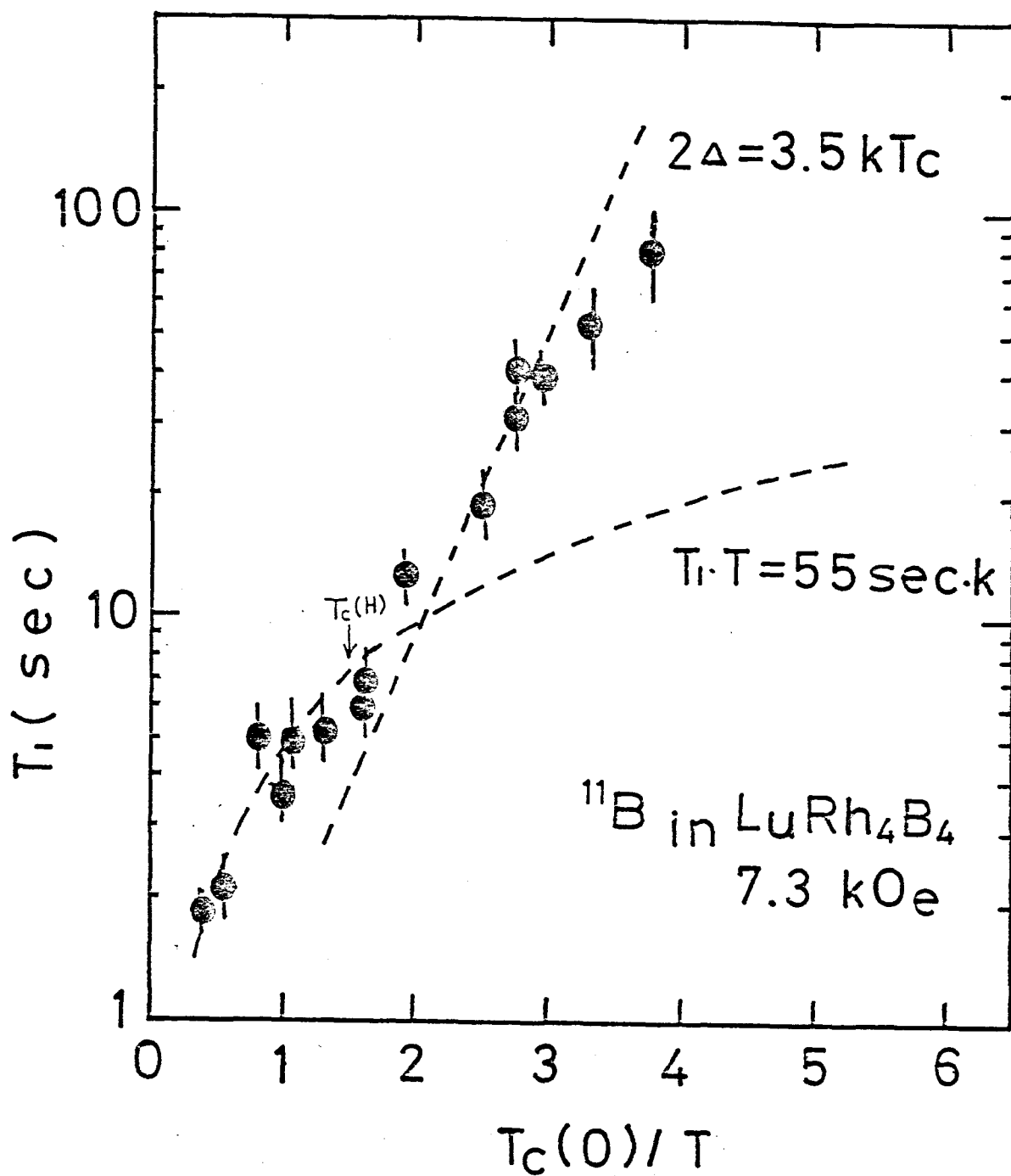Fig.6 Temperature dependence of T_1 of ^{11}B in LuRh$_4$B$_4$. The arrow indicates the T_c(H) at 7.3 kOe.

Table 3

Comparison of calculated and observed T_1 in $LuRh_4B_4$ and YRh_4B_4. $N(E_F)$ is in units of (state/eV $\cdot$ atom $\cdot$ spin) H_{hf} is in (10^6 Oe) and $(T_1T)^{-1}$ is in (sec$\cdot$ K)$^{-1}$.

	$N_s(E_F)$	$N_p(E_F)$	$N_d(E_F)$	H_s	H^p_{orb}	H^d_{orb}	H^d_{cp}	$(T_1T)^{-1}_{cal}$	$(T_1T)^{-1}_{exp}$
^{89}Y	0 [a]	0.037 [a]	0.35 [a]	8.8 [b]	1.29 [b]	0.16 [b]	-0.21 [b]	f=1 0.0087	0.011
^{103}Rh	0.018 [a]	0.074 [a]	0.41 [a]	9.8 [c]	2.5 [c]	0.98 [c]	-0.12 [c]	(f=3/5) (0.0085) f=1 0.025 (f=3/5) (0.039)	0.04
^{11}B	0.009 [a]			1.0 [d]				0.0044	0.022 [e] 0.018

a) reference 8)

b) reference 14)

c) reference 15)

d) reference 16)

e) reference 13)

(1-2) NMR in superconducting mixed state

In type II superconductor the field penetration λ is much larger than the superconducting coherent length ξ. ($\xi << \lambda$) Then the surface energy of a wall separating normal and superconducting region becomes negative. In order to maximize the surface to volume ratio for the normal region , the normal and superconducting regions are finely divided and normal region forms a filament of small diameter. Each filament has a hard core of radius ξ, where the superconducting electron density is reduced as shown in Fig.7. The field is maximum at the center of the filament but extends to the super-conducting region with a distance λ.

In the intermediate fields $H_{c1} \ll H \ll H_{c2}$, where the vortices (filaments of normal regions) form a dense lattice. The detailed calculation shows that the most favorable arrangement is triangle lattice.[17] Then the magnetic flux density B is

$$B = \phi_0 n_L = 2/\sqrt{3} \cdot \phi_0/d^2 \qquad (6)$$

where ϕ_0 is one quantum of flux ,

$$\phi_0 = ch/2e$$
$$= 2 \times 10^{-7} \text{ G cm}^2 \qquad (7)$$

d is the distance between the nearest neighbor filaments and n_L is the number of flux per unit area.

Thus field penetrates into the superconducting state. The field distribution is expressed by mean square root of   field.

$$\Delta H = (<H^2> - <H>^2)^{1/2}$$
$$= \frac{B}{\sqrt{4\pi}} \frac{d}{\lambda} (1 + (\frac{2\pi\lambda}{d})^2)^{-1/2} \qquad (8)$$

Figure 5-2 shows ^{11}B NMR of $\pm 1/2$ transition of quadrupole split lines in superconducting mixed state of the non-magnetic compound $LuRh_4B_4$. The excess broadening compared with/that in the normal state is observed. This line broadening is associated with the field inhomogeneity ΔH of eq.8.   By using this equation λ is estimated to be 1000Å in $LuRh_4B_4$. The negative shift of the spectrum is associated with diamagnetism of superconductivity.
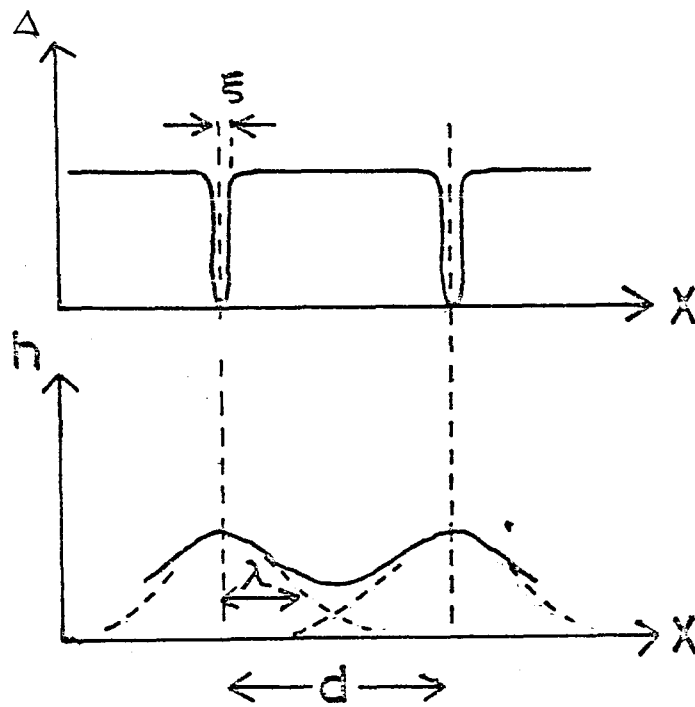
Fig.7 Structure of vortex line in a type II superconductor. The

magnetic field is maximum near the center of the vortex line. Going

outwards, h decreases because of the screening in an electromagnetic

region of radius $\simeq \lambda$. Owing to the superposition of nearest

neighbor contribution the field penetrates into the superconducting

state. On the other hand superconducting electron density is

reduced only in a core region of radius ξ .

T_1 in BCS superconductor is described in general form [18]

$$\frac{T_1^N}{T_1^S} = \frac{2}{k_B T} \cdot \int \frac{(E\ E' + \Delta^2)\ f(E)\ (1 - f(E'))}{[(E^2 - \Delta^2)(E'^2 - \Delta^2)]^{1/2}}\ d E \qquad (9)$$

$$E' = E \pm \hbar \omega_n$$

where Δ is the superconducting energy gap, ω_n is rf frequency and $f(E)$ is the Fermi-Dirac distribution function of the quasiparticle excitation energy E. This relaxation due to the nuclear hyperfine interaction with the conduction electrons shows an enhancement just below T_s due to the sharp peak in the density of states at the gap edge and an exponential behavior on temperature at low temperature with $2\Delta = 3.5\ k_B T_s$.

In $LuRh_4B_4$ T_1 of ^{11}B in the superconducting state was measured. The result is shown in Fig.6. T_1 changes exponentially as $\exp(\Delta/k_B T)$ with $2\Delta = 3.5\ k_B T_s$ ($T_s = 11$ K). The energy gap obtained from T_1 is just the same value as obtained by BCS theory. This means $LuRh_4B_4$ is a weak coupling superconductor.

(2) NMR study of RERh$_4$B$_4$ compound

(RE is magnetic ion) - Knight shift measurement

RERh$_4$B$_4$ compounds exhibit complex magnetic properties. For example, Dy compound has the highest T$_m$(11.2 K) in the series of simple ferromagnetic compound from Gd to Ho, as shown in Fig.8.
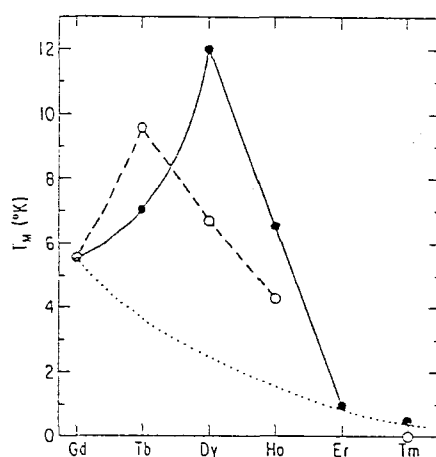

Fig.8   Magnetic transition temperature. closed circle: the observed value,

dotted line: the value predicted by deGennes rule ,

open circle: the value obtained by the molecular field model with R$_2^0$ crystal field parameter.

In order to understand the magnetic properties microscopically we performed NMR study in   RERh$_4$B$_4$ compound. (RE = Nd, Sm, Gd, Tb, Dy, Ho, Er and Tm)

(2-1) Knight shift of ^{11}B

We measured the Knight shift of ^{11}B to see the variation of the conduction electron spin polarization with RE in dense RERh$_4$B$_4$ system. In the paramagnetic state the localized moments induce a uniform conduction electron spin polarization, which yields the Knight shift of the non-magnetic nuclear species.

The typical spectra obtained for RE = Gd, Sm and Tm are shown in Fig.9-1, Fig.10-1 and Fig.11 respectively. These NMR spectra are anisotropic in paramagnetic state. We analyzed the spectra by using the conventional form for isotropic and anisotropic shift ,
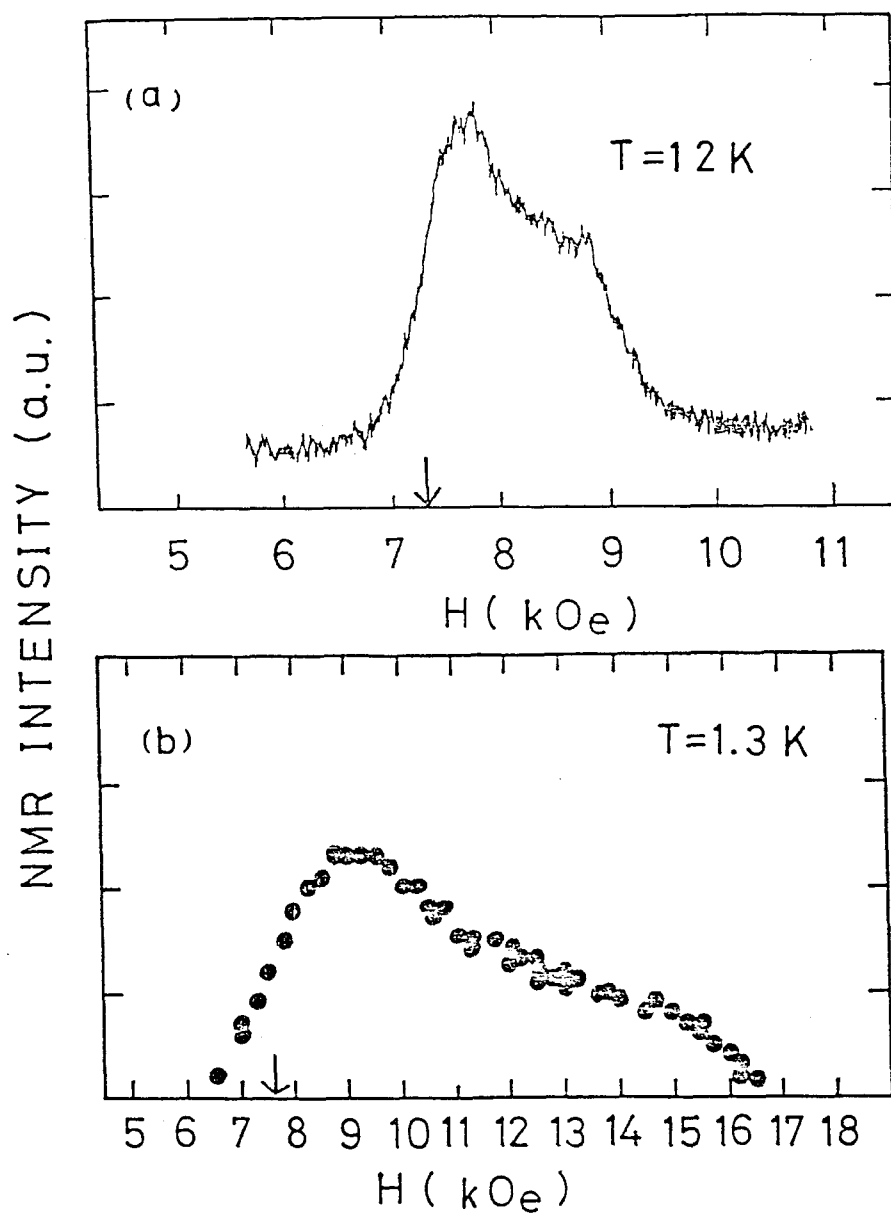
Fig. 9-1   NMR spectrum of [11]B in GdRh$_4$B$_4$ at T= 12K and f = 10.0MHz.   The system
is in paramagnetic state, the arrow means K = 0.

Fig. 9-2   NMR spectrum of [11]B in GdRh$_4$B$_4$ at T = 1.3K and f= 10.0 MHz.   The
system is in ferromagnetically ordered state.
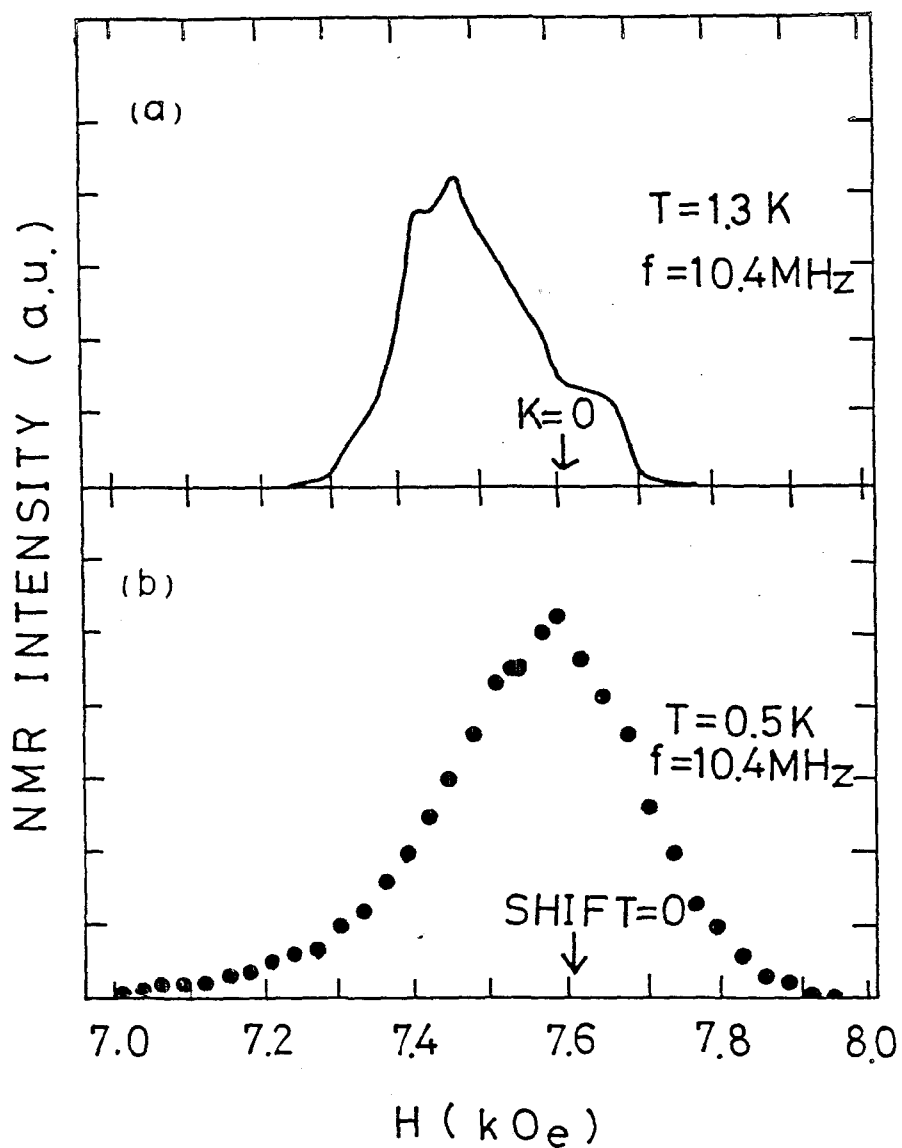
Fig. 10.1 NMR spectrum of [11]B in SmRh$_4$B$_4$ at T= 1.3 K and f = 10.4 MHz. The system is in paramagnetic and normal state.

Fig. 10.2 NMR spectrum of [11]B in SmRh$_4$B$_4$ at T = 0.5K and f= 10.4 MHz. The system is in antiferromagnetic and normal state.
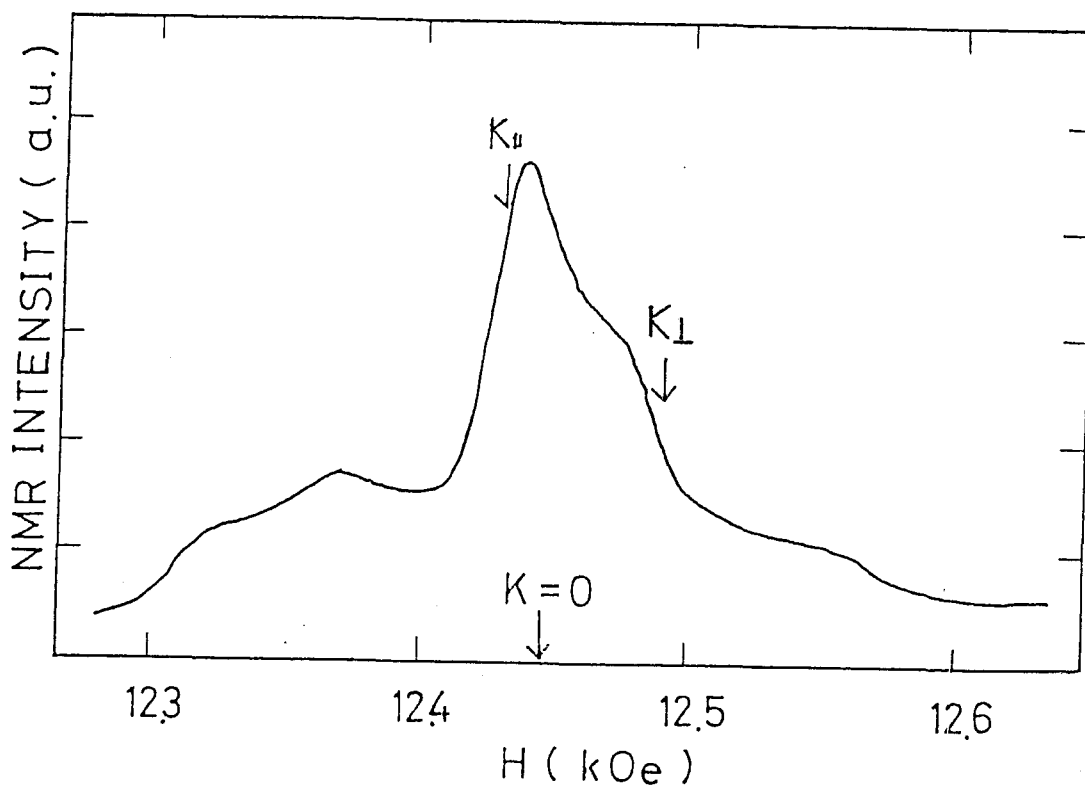
Fig. 11 NMR spectrum of ^{11}B in $TmRh_4B_4$ at T= 300K and f=17.0MHz.

$$K = K_{iso} + 1/2 \cdot K_{anis} (3 \cos^2\theta - 1) \qquad\qquad (10)$$

$K(\theta=90°)$ is determined at 85% of the peak height and $K(\theta=0°)$ is determined at 50%
of the shoulder height as the spectrum has an extra Gaussian broadening.

By using $K(\theta=90°)$, $K(\theta=0°)$ and eq. 10 , K_{iso} and K_{anis} are determined .

The isotropic and anisotropic hyperfine coupling constants, A_{iso} and A_{anis} are

obtained from the Knight shift and the susceptibility data, χ_f.

$$K_{iso} = A_{iso} \cdot \chi_f$$

$$(11)$$

$$K_{anis} = A_{anis} \cdot \chi_f$$

In Gd and Sm compound K vs χ plot with temperature as an implicit

parameter is shown in Fig.12 and Fig.13 respectively.
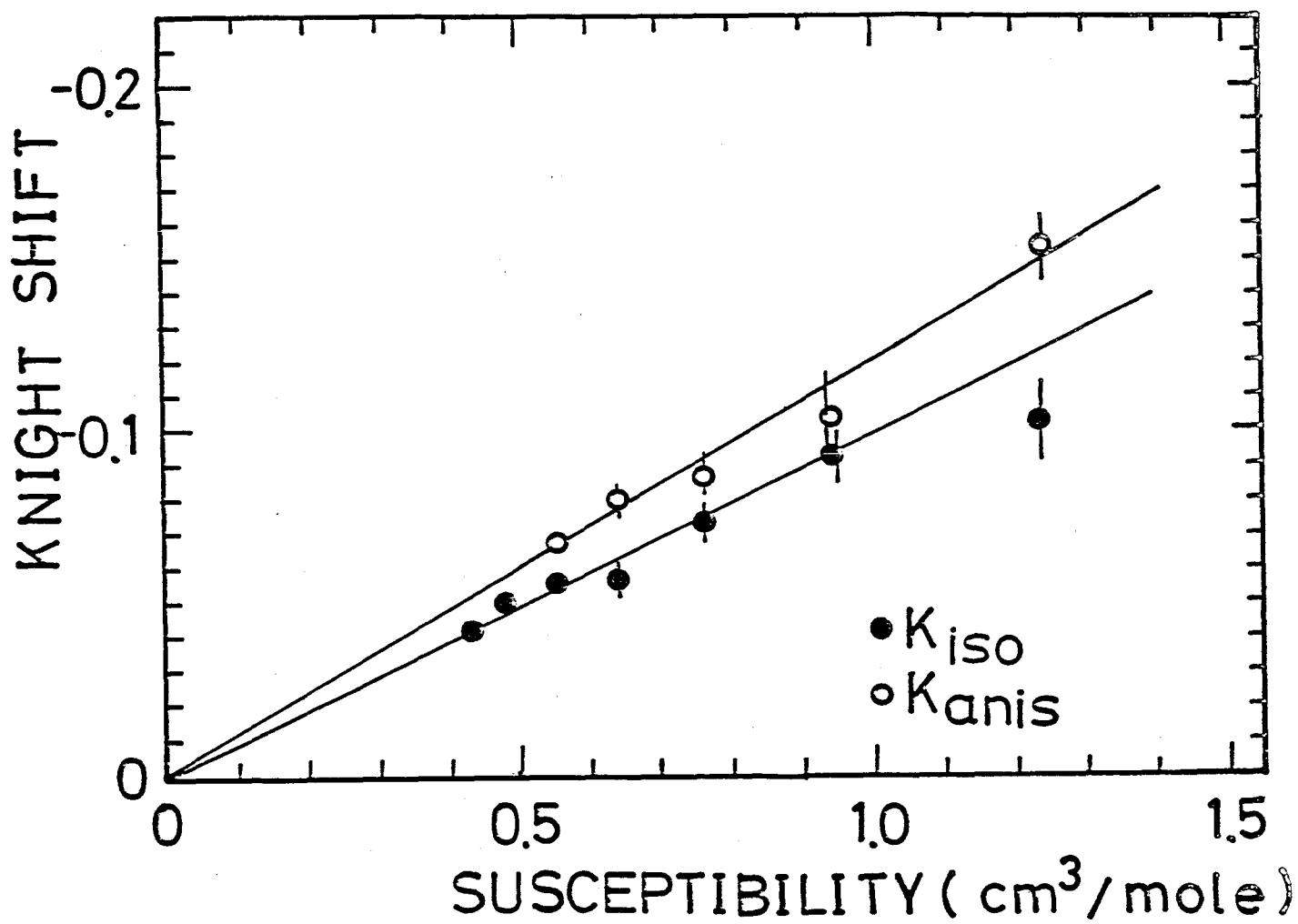
Fig. 12 Isotropic and anisotropic Knight shift of ^{11}B in $GdRh_4B_4$ vs susceptibility.
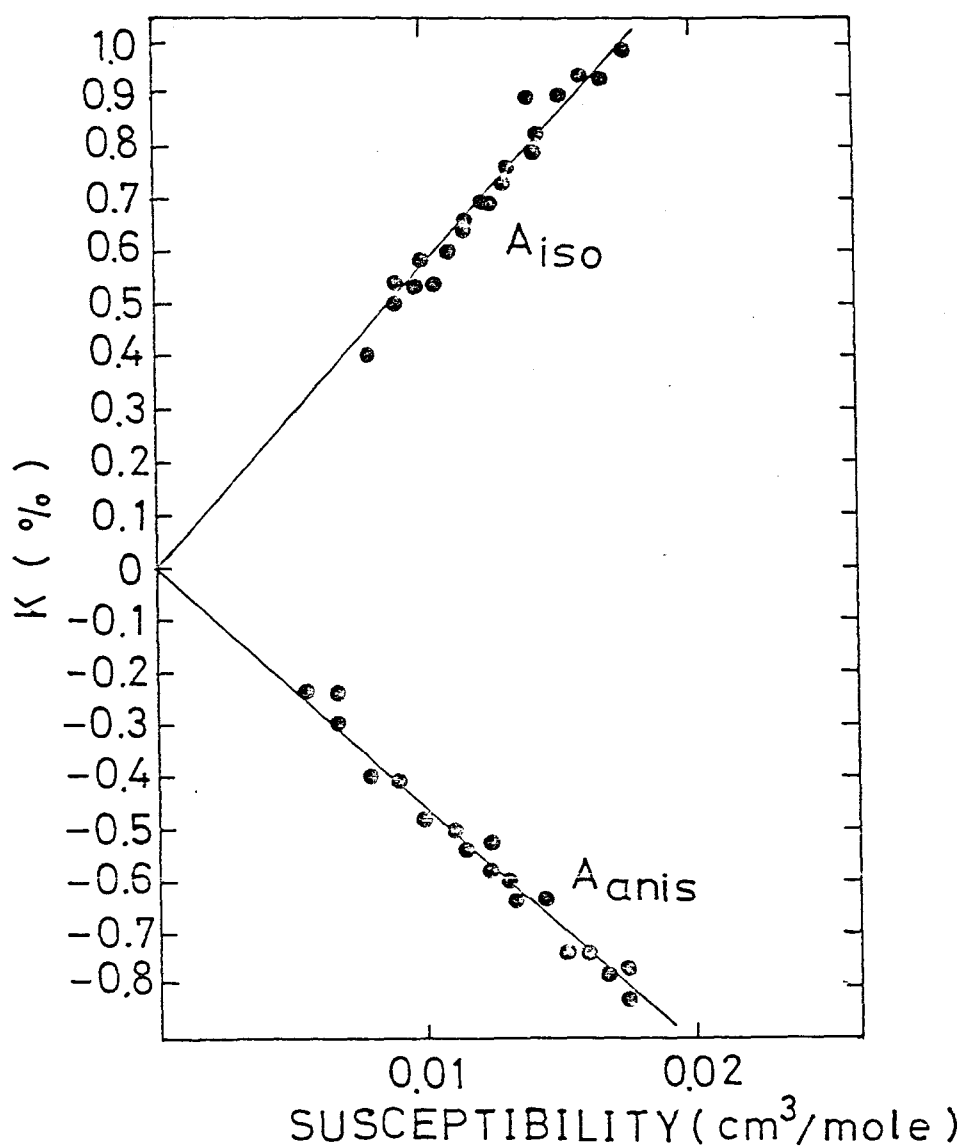
Fig. 13   Isotropic and anisotropic   Knight shift of ^{11}B in $SmRh_4B_4$ vs
susceptibility.

In Nd, Tb, Dy, Ho, Er and Tm compound   Knight shifts are obtained at 300K
With the susceptibility data, the hyperfine coupling constants are obtained
in Dy, Ho, Er, Tm and Nd compounds.   For RE = Tb we used the free atom
value for the effective moment, as there is no susceptibility datum.   The
obtained   coupling constants are shown in Fig.14 and Fig.15 respectively.

The isotropic shifts are all negative for the heavy RE and positive for the light RE. This shift is induced by the conduction electron spin polarization at B site. Especially conduction electron, which has s-symmetry at B site is responsible for this shift. We can evaluate the conduction electron spin polarization by using a simplified uniform polarized model.[19]

$$K_{iso} = A_{iso} \cdot \chi_f$$

$$A_{iso} = \frac{g_J - 1}{g_J} \cdot \frac{4 \, J_{sf} \, N_s(E_F) \, H_S}{9\mu_B}$$

(12)

where g_J is the Landé g factor, μ_B is Bohr magneton , χ_f is the thermal averaged value of RE moments in external field, J_{sf} is the exchange interaction between the RE moment and the conduction electron and H_s is the atomic hyperfine field of ^{11}B. J_{sf} means the exchange interaction with s-electron at RE site in uniform polarized model. However more precisely d-electron spin polarization at RE site also contributes to the conduction electron spin polarization which has s-symmetry at B site.

As shown in Fig.14, A_{iso} is well explained by

$$A_{iso} = \frac{g_J - 1}{g_J} \cdot 2 \, A_{iso}(Gd)$$

(13)

$$A_{iso}(Gd) = -550 \; Oe/\mu_B$$

This means that $J_{sf}N_s(E_F)$ is nearly same , or the conduction electron spin polarization which is induced by unit spin is nearly same for all $RERh_4B_4$. $J_{sf}N_s(E_F)$ is obtained to be -2.4×10^{-3} state/ atom spin, where $H_s = 1.0\times10^6$ Oe is assumed.[16]
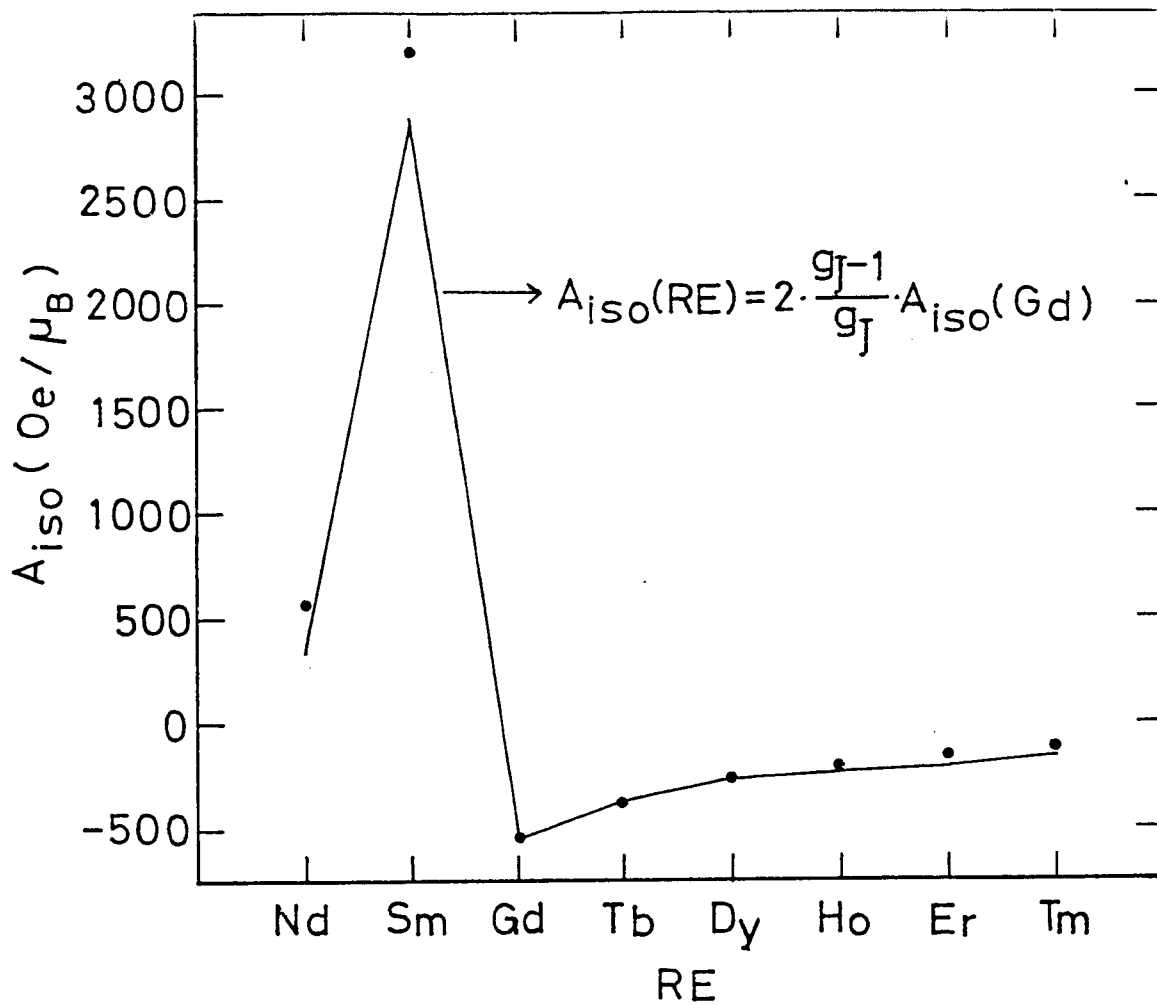
Fig. 14 A_{iso} of ^{11}B in $RERh_4B_4$. The solid line represents the isotropic hyperfine coupling const., which is normalized by the $A_{iso}($ Gd)

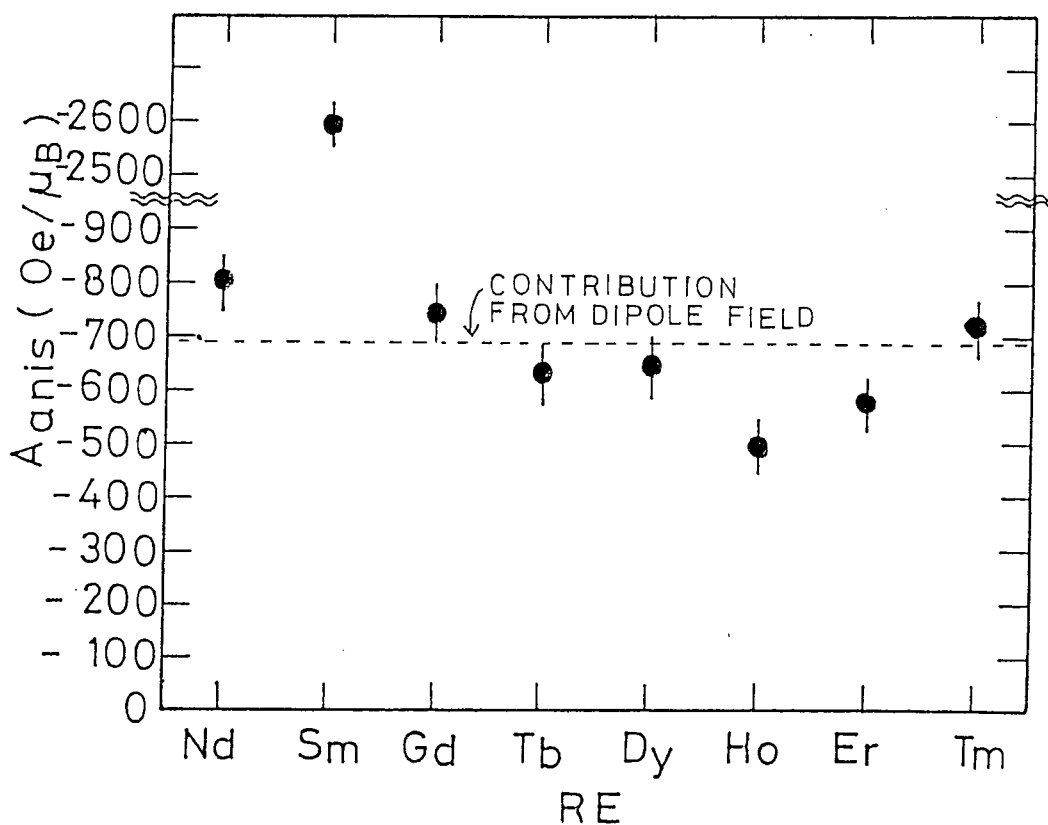In the figure: $A_{iso}(RE) = 2 \cdot \dfrac{g_J - 1}{g_J} \cdot A_{iso}(Gd)$

Fig. 15 A_{anis} of ^{11}B in $RERh_4B_4$. The dashed line represents the contribution from the dipole field.

CONTRIBUTION FROM DIPOLE FIELD

If T_m is determined only by RKKY interaction, T_m should be proportional to the de Gennes factor $G = (g_J-1)^2 J(J+1)$, where J is the total angular momentum. The de Gennes factor can be derived in the simplest of molecular field model.

$$\mathcal{H}_{exch} = -2 \mathcal{J}(g_j - 1)^2 J_z \langle J_z \rangle$$

where z-axis is the direction of the magnetic moment. $\mathcal{J}'$ is the effective exchange integral between RE ions. Then the magnetic transition temperature T_0 is

$$T_0 = 2 \mathcal{J}(g_j - 1)^2 J(J+1)/3 \tag{14}$$

$$\mathcal{J} = \frac{2z_0}{3k_B} \mathcal{J}'$$

where z_0 is the number of interacting RE ions.

As shown in Fig.8, however, Dy compound has the highest T_m. This means that T_m is determined not only by RKKY interaction but also by other contribution such as the crystal field effect (CFE). Indeed, recently, Shenoy has taken into account the CFE contribution[15]. When the CFE splits the J_z state significantly with respect to $k_B T_0$, CFE terms should be added to the exchange Hamiltonian. That is

$$\mathcal{H} = -2 \mathcal{J}'(g_j - 1)^2 J_z \langle J_z \rangle + B_2^0 [3J_z^2 - J(J+1)] \tag{15}$$

When the ordering is along c-axis this leads to an ordering temperature T_m given by

$$T_m = 2 \mathcal{J}(g_j - 1)^2 \cdot \frac{\sum_{J_z} J_z^2 \exp(-3B_2^0 J_z^2/T_m)}{\sum_{J_z} \exp(-3B_2^0 J_z^2/ T_m)} \tag{16}$$

The transition temperature of the Gd compound can be used to fix a value for the exchange parameter, $\mathcal{J}'$, because Gd, an L=0 ion, is not affected by CFE. For the rest of the series, the RE dependent B_2^0 parameter can be expressed for each RE.

$$B_2^0 = \alpha_2 A_2^0 \langle r^2 \rangle \tag{17}$$

where α_2 is the Stevens factor for each RE, [20] $<r^2>$ is the second moment of the 4-f radial wave function. [21] A_2^O is a value related to the charge distribution. Shenoy et al measured the electronic field gradient at Gd nucleus by Mössbauer effect and determined A_2^O. [22] B_2^O for each RE is estimated by using eq.17, and each T_m is also calculated by using eq.16. The result is shown in Fig.8. It is shown that the crystal field effect causes significant deviation from de-Gennes scaling. The calculated value becomes close to the experimental value.

The anisotropic coupling constant is shown in Fig.15. K_{anis}, which is induced by the dipole field from RE magnetic moments, is expressed as [19]

$$K_{anis} = -11.1 \cdot \frac{\chi_f}{a^3} \qquad (18)$$

where a is a lattice parameter. By using each χ_f and lattice constant, K_{anis} is calculated and is shown in Fig.15. A_{anis}(RE) is expressed by the dipolar contribution except RE=Sm. In $SmRh_4B_4$, Knight shift is measured at low temperature (1.2K $\sim$ 10K), where K_{anis} is about 4.6 times larger than the dipolar contribution. This suggests that the anisotropy of the static susceptibility also induces the anisotropic shift via the uniform spin polarization,

$$K_{anis} = A_{iso} \cdot \chi_{anis}$$
$$\chi_{anis} = 2/3 \cdot (\chi_{//} - \chi_\perp) \qquad (19)$$

where $\chi_{//}$ and $\chi_\perp$ are parallel and perpendicular component of χ to the tetragonal c-axis respectively. In order to explain the anisotropy by the contribution from χ_{anis}, we have to take $\chi_\perp / \chi_{//}$ to be 7.5. ($\chi_\perp$ is much larger than $\chi_{//}$) As B_2^O for Sm^{3+} is negative in $SmRh_4B_4$, the easy axis of Sm moments may be in a-b plane and anisotropy of χ appears. On the other hand in other $RERh_4B_4$, the Knight shift is measured at 300K and neary all the energy levels of J_z are thermaly excited. Then K_{anis} may be explained only by the contribution from the dipole field.

(2- 2) Knight shift of ^{103}Rh in SmRh$_4$B$_4$

In Sm compound, we observed ^{103}Rh NMR in the paramagnetic state. The spin echo spectrum at 2.25 K is shown in Fig.16. The spectrum is broadened and the anisotropy of the spectrum is smeared by rf pulse. The shift is determined at the peak of the spectrum, and is shown in Fig.17 against the susceptibility data.[23] K_{iso} is linear in $\chi_f(T)$ and the slope in K_{iso} vs χ plot yields the hyperfine coupling constant of ^{103}Rh, $[A_{iso}(S_m)]_{Rh} = 1$ kOe. The observed hyperfine field is a sum of s- and d- part of contribution. We tentatively try to separate the conduction electron spin polarization. Assuming that the difference of $(A_{iso})_{Rh}^s$ and $[A_{iso}]_B^s$ is owing to the difference of the hyperfine coupling const. and the density of states , we estimate $[A_{iso}(Sm)]_{Rh}^s$ as

$$[A_{iso}(Sm)]_{Rh}^s = [A_{iso}(Sm)]_B^s \cdot \frac{[N_s(E_F)]_{Rh}^s}{[N_s(E_F)]_B^s} \cdot \frac{(H_{Rh}^s)_{atom}}{(H_B^s)_{atom}} \qquad (20)$$

$$= 31 \text{ kOe}/\mu_B$$

where $(H_{Rh}^s)_{atom} = 4.79 \times 10^6$ Oe [24] and $(H_B^s)_{atom} = 1.0 \times 10^6$ Oe [16]. Then the contribution from d- electron is estimated as

$$[A_{iso}(Sm)]_{Rh}^d = [A_{iso}(Sm)]_{Rh} - [A_{iso}(Sm)]_{Rh}^s \qquad (21)$$

$$= - 30 \text{ kOe}/\mu_B$$

$[A_{iso}]_{Rh}^s$ and $[A_{iso}]_{Rh}^d$ are much larger than the observed coupling constant and are nearly cancelled. In a uniform polarized model (eq.12), $J_{df}N_d(E_F)$ is estimated as

$$J_{df} N_d(E_F) = - 0.23 \text{ state/ atom spin} \quad ,$$

where $(H_{Rh})_{cp}^d = - 0.12 \times 10^6$ is assumed.

This value is larger than $JN(E_F) \simeq 0.1$ state/atom spin at RE site obtained from Korringa fluctuation of RE moments. If $(A_{iso})_{Rh}^s$ is smaller than the expected value. $(A_{iso})_{Rh}^d$ and $J_{df}N_d(E_F)$ at Rh site becomes smaller. However $(A_{iso})_{Rh}^s$ has at least the same magnitude as $(A_{iso})_{Rh}^d$. Even then $J_{df}N_d(E_F)$ at Rh site is an order of magnitude larger than that found in Chevrel phase compounds.
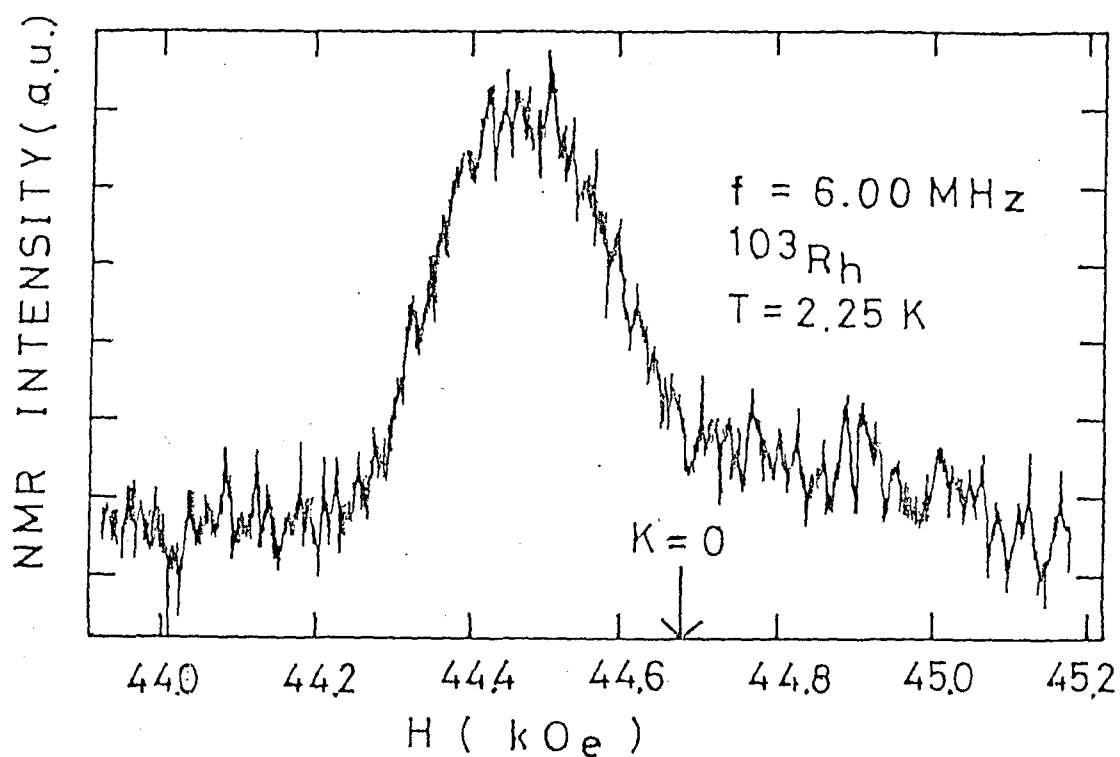
Fig.16 NMR spectrum of ^{103}Rh in SmRh$_4$B$_4$. The positive shift appears.

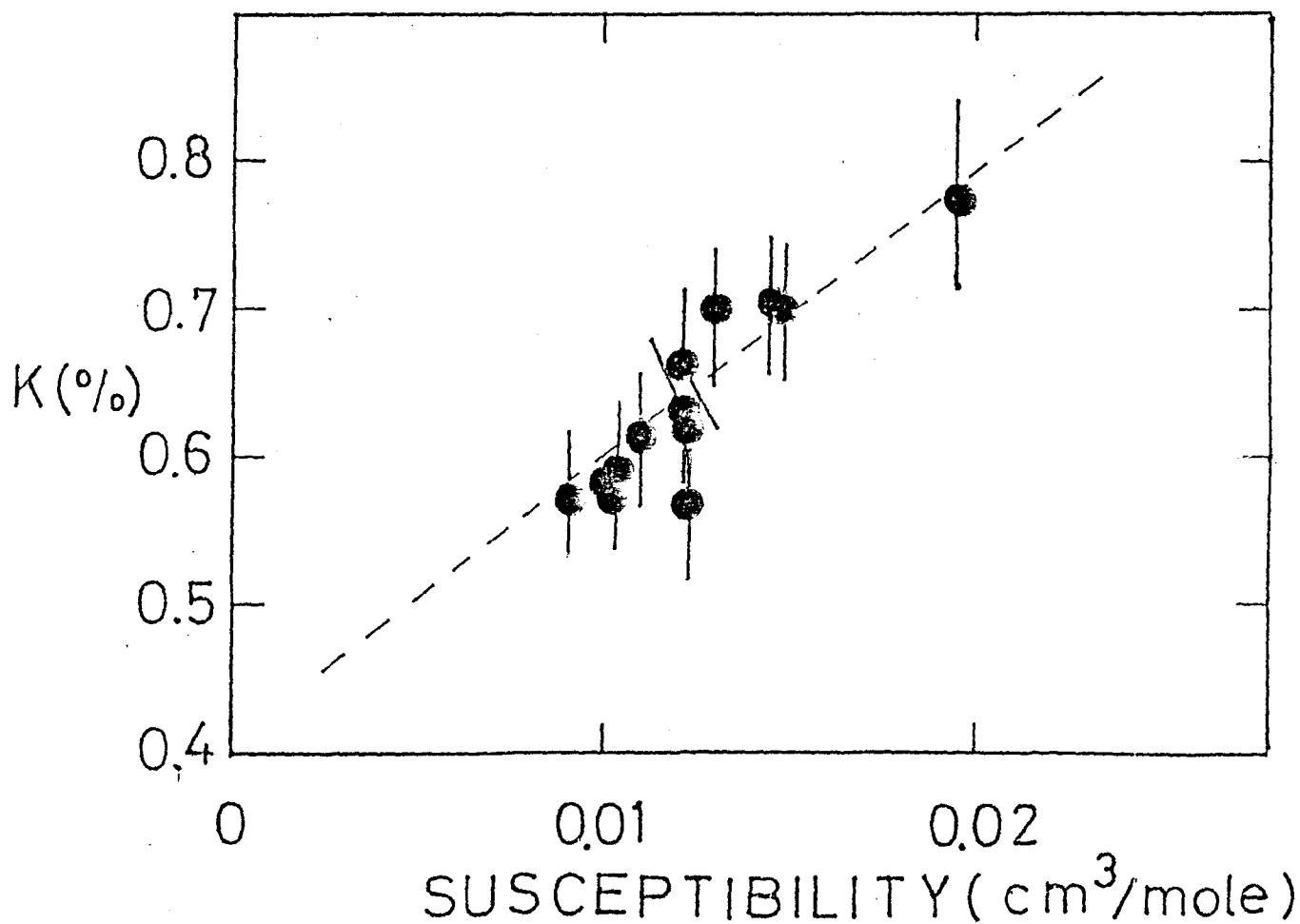Fig.17 The isotropic shift of ^{103}Rh in SmRh$_4$B$_4$ vs susceptibility.

(3) NMR spectra of ^{11}B in the magnetically ordered state

(ferromagnetic compounds)

In the magnetically ordered state, zero field NMR of ^{11}B was observed in ferromagnetic compounds.[25] We obtain information about the magnetic structure in these compounds using the hyperfine field data.

The hyperfine field of ^{11}B in ferromagnetic compound may be expressed as a sum of the dipole field from the surrounding RE ions, the hyperfine field due to the conduction electron spin polarization and the Lorentz field due to the magnetization of RE moments .

$$H_{hf} = H_{dip} + H_{cond} + H_L \qquad\qquad (22)$$

Each contribution is calculated by the following procedure. The magnetic moments are directed to c-axis for $HoRh_4B_4$ and ab plane for $ErRh_4B_4$ according to the neutron diffraction measurement. Assuming that the magnetic moments in Gd, Tb and Dy compounds are aligned along c-axis, one can calculate the hyperfine fields. The values of the magnetic moments in Dy-, Ho and Gd- compound are found to be $9.2\mu_B$ from Mössbauer effect by Shenoy et al.,[26] $8.7\mu_B$ from neutron diffraction by Mook et al[27] and $7\mu_B$ respectively. As for the classical dipole field at B site, one calculates the value from the first nearest-neighbor RE site in the distance of about 70 Å around B. H_{cond} was calculated by using $(g_J-1)J$ of RE and the hyperfine coupling constant for ^{11}B, which was obtained from the Knight shift measurement. The Lorentz field $4/3 \cdot \pi M$ was obtained by using the measured magnetic moment and the lattice constant. Each component contributing to H_{hf} is shown schematically with its direction in Fig.18. The measured H_{hf}, the total calculated H_{hf}, the dipole fields parallel and perpendicular to the magnetic moment $H_{dip\parallel}$ and $H_{dip\perp}$, H_L and H_{cond} are shown in Table 4. As shown in this table , the calculated H_{hf} of these compounds are in reasonable agreement with the measured values.
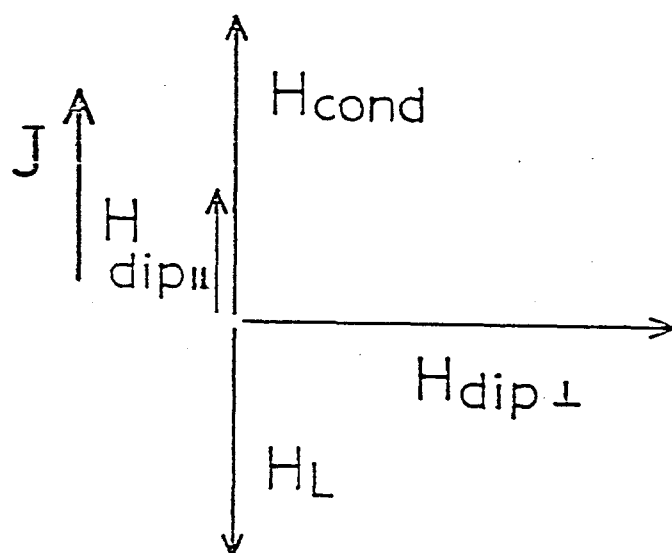
Fig. 18 The direction of each component of H_{hf} at B site relative to the total

angular momentum J. The marks of $H_{dip\,\parallel}$ and $H_{dip\perp}$ show the parallel and

perpendicular component with respect to magnetization

Table 4

The measured H_{hf} and the calculated H_{hf} at B site.

R_E	$H_{hf\ meas}$ (kOe)	$H_{hf\ calc}$ (kOe)	$H_{dip\perp}$	$H_{dip\,\parallel}$	H_{cond}	H_L
Gd	3.15	3.55	3.21	0.28	3.86	2.62
Dy	4.69	4.26	4.25	0.38	2.76	3.44
Ho	4.61	4.56	4.04	0.35	2.21	3.25
Tb	3.9					

(4) Nuclear spin lattice relaxation rates of ^{11}B

The fluctuation of RE moments enhances T_1^{-1} of ^{11}B through the RKKY coupling and the magnetic dipole coupling between RE spin and ^{11}B. Then T_1 of ^{11}B provides informations about the origin of RE spin fluctuation: the s-f exchange interaction of RE spin and conduction electrons, the indirect coupling of the each RE spin and also the crystal field effect on the RE spin.

□ NdRh$_4$B$_4$
● SmRh$_4$B$_4$
▽ GdRh$_4$B$_4$
▼ TbRh$_4$B$_4$
● DyRh$_4$B$_4$
■ HoRh$_4$B$_4$
△ ErRh$_4$B$_4$
○ TmRh$_4$B$_4$

Fig.19 The temperature dependence of T_1^{-1} of ^{11}B in RERh$_4$B$_4$.
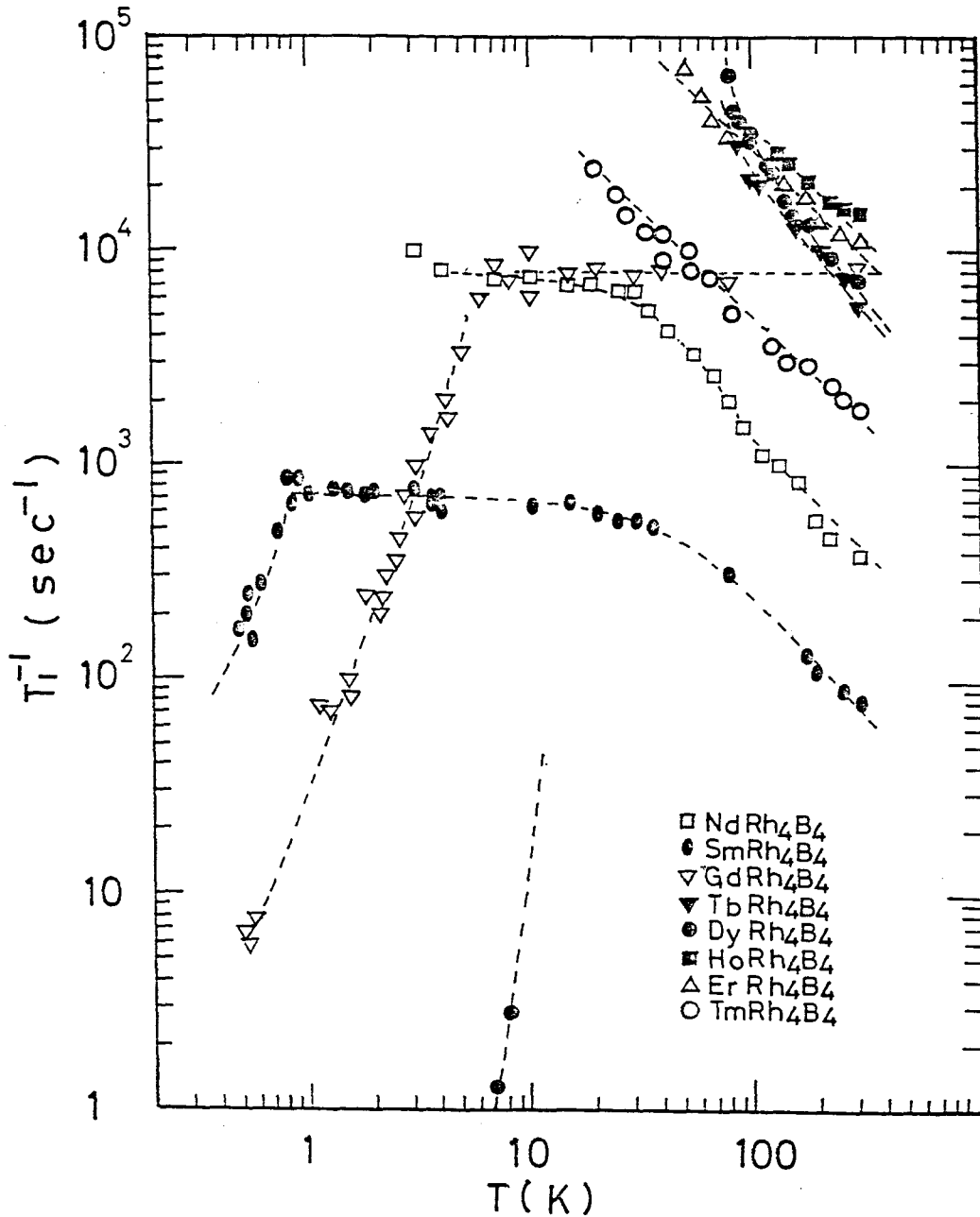
T_1 is expressed as

$$T_1^{-1} \propto \gamma_n^2 \cdot H_{loc}^2 \cdot \frac{\tau}{1 + (\omega_n \tau)^2} \qquad (23)$$

where γ_n is the gyromagnetic ratio of ^{11}B, H_{loc} is the coupling of B nucleus and RE spin (RKKY and/or dipole coupling), ω_n is the nuclear Larmor frequency and τ is the electronic spin correlation time, which is determined by the Korringa spin fluctuation of RE spin or RKKY indirect coupling of RE spin.

The temperature dependence of T_1 of ^{11}B in $RERh_4B_4$ is shown in Fig.19. At high temperature T_1^{-1} decreases with increasing temperature (except $GdRh_4B_4$). T_1 is nearly proportional to T and field dependence is not observed. This behavior is widely seen in most of the compounds (except $GdRh_4B_4$). In this case the Korringa relaxation of the electronic spins via the s-f exchange interaction governs the RE spin fluctuation.

The temperature dependence of T_1 at low temperature depends on RE species. In Gd-, Nd-, and Sm- based compound T_1 is temperature independent. This behavior suggests that the exchange interaction between Gd spins (RKKY coupling) is responsible for the electronic spin correlation time, τ.

In Dy- based compound, T_1^{-1} increases with decreasing temperature and then decreases exponentially at low temperature,

$$T_1^{-1} \propto \exp(- \Delta / k_B T) \quad \text{with} \ \Delta \simeq 130K$$

This means that τ changes in proportional to $\exp(-\Delta/k_B T)$ at low temperature.

As discussed in the previous section RE ion experiences the relatively large crystal field in $RERh_4B_4$. For example, the Schottky anomalies in specific heat indicate the crystal field effect on RE ions. T_1 is also affected by the crystal field effect and is especially sensitive to the ground state at low temperature. In Dy-based compound, the RE spin fluctuation is suppressed by the crystal field.

(4-1) T_1 of ^{11}B in $GdRh_4B_4$

First we consider T_1 in $GdRh_4B_4$. As Gd, an L=0 ion, is not affected by the crystal field effect, the behavior of T_1 is simplest in $RERh_4B_4$. In the paramagnetic state T_1 is nearly temperature independent between 8K and 300K, being 125μsec which is smaller by about four orders of magnitude compared with that in non-magnetic $LuRh_4B_4$. (T_1T = 55secK in $LuRh_4B_4$. This value is due to the direct relaxation to the conduction electron at B site.) This means that the exchange interaction between Gd spins to be responsible for the fluctuation of the Gd spins. T_1 of ^{11}B due to the magnetic dipole interaction between Gd^{3+} spin and ^{11}B nuclear spin is expressed as [28]

$$T_1^{-1} = \frac{\sqrt{2\pi}\ \gamma_e^2 \gamma_n^2 \bar{h}^2}{6\ \omega_e} \cdot S(S+1) \cdot \sum_1 r_1^{-6} [\ F_1(\alpha\ \beta\ \gamma) + F_1'(\alpha\ \beta\ \gamma)]\qquad (24)$$

where ω_e is the exchange frequency, γ_e is the gyromagnetic ratio of the electrons, r_1 is the distance between ^{11}B and Gd ion and S is the spin number. F_1 and F_1' are the functions of the direction cosine of the local magnetic field of the nucleus, α, β, γ. We replace F_1 and F_1' by their directional average, $<F_1>$ and $<F_1'>$, as they are not so sensitive to the direction. Then eq. 24 is expressed as

$$T_1^{-1} = \frac{2\ \sqrt{2\pi}\ \gamma_e'^2\ \gamma_n^2 \bar{h}^2}{3\ \omega_e} S(S+1) \sum_1 r_1^{-6}\ .\qquad (25)$$

We estimate ω_e from the Curie temperature T_c. Gd spin is in s-state, not affected by the crystal field effect. The contribution to T_c from the dipole coupling is order of 0.25K(M =7μ_B, r=5Å), which is smaller than the experimental value. Then T_c is determined mainly by RKKY exchange coupling.

$$(\bar{h}\ \omega_e)^2 = \frac{1}{6z} \cdot \frac{(3k_B\ T_c)^2}{S(S+1)}\qquad (26)$$

Putting eq.26 into eq.25, T_1 is estimated to be 25μsec.

In addition to the dipole coupling, the coupling between [11]B and Gd spin via the conduction electron spin polarization also contributes to T_1^{-1}. This value may be estimated by the relation [29]

$$T_1^{-1} = \sqrt{2\pi} \sum_i \left(\frac{A_i}{\hbar}\right)^2 \frac{S(S+1)}{3\omega_e} \qquad (27)$$

where A_i is a hyperfine coupling constant between [11]B and i-th Gd spin via the conduction electron spin polarization. Although we have no knowledge about A_i, we tentatively try to estimate A_i from the isotropic Knight shift. Assuming roughly that T_1 is caused by nearest neighbor 3 Gd moments, A_i is estimated as 3.3×10^{-21} erg and T_1 is calculated to be 167μsec, which is longer than the value due to the dipole interaction. Thus in $GdRh_4B_4$ T_1 seems to be governed by the fluctuations of the dipole field from the Gd spins.

When the system sets into ferromagnetic state, T_1^{-1} decreases rapidly with decreasing temperature, as the spin fluctuations are suppressed.
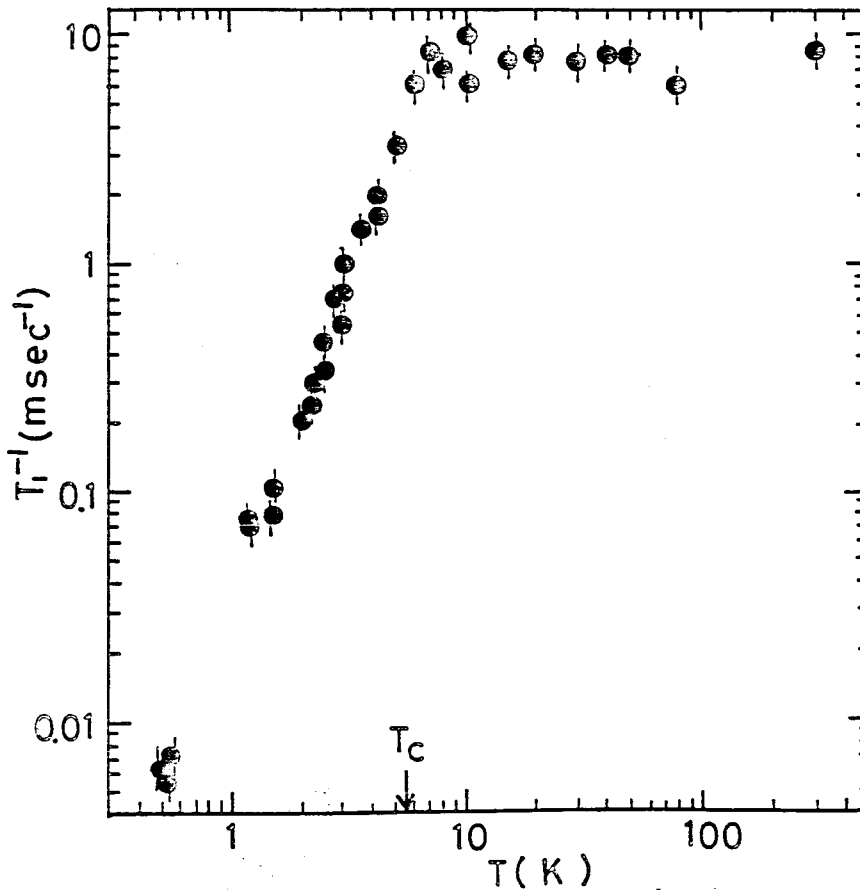

Fig. 20 Temperature dependence of T_1^{-1} of [11]B in $GdRh_4B_4$.

(4-2) T_1 of ^{11}B in $RERh_4B_4$ —— high temperature

As shown in Fig.19 T_1 is nearly proportional to T at high temperature
in most of the compounds. In this case the Korringa relaxation of the
electronic spins via the s-f exchange interaction is responsible for the
fluctuation of RE moment. The relaxation rate W is expressed as [30]

$$ W = \frac{2\pi}{\hbar} \cdot (g_j - 1)^2 [J\ N(E_F)]^2\ k_B T \qquad (28) $$

where J is the s-f and/or d-f exchange interaction, and $N(E_F)$ is the density
of state at RE site.

In this region T_1 due to the dipole coupling between RE and ^{11}B
is expressed as

$$ T_1^{-1} = \frac{2\gamma_e^2 \gamma_n^2 \hbar^2}{3\ W}\ g_j^2 J(J+1)\ \sum_1 r_1^{-6} \qquad , \qquad (29) $$

$$ \propto \frac{g_j^2 J(J+1)}{(g_j-1)^2} \qquad , $$

while that due to RKKY coupling is expressed as

$$ T_1^{-1} = \frac{S(S+1)}{3\ W} \cdot \sum_1 (\frac{A_1}{\hbar})^2 \qquad , \qquad (30) $$

$$ \propto J(J + 1) \qquad , $$

The RE dependence of the observed relaxation rate is shown
in Fig.21. The RE dependence of $(T_1)_{dipole}$ and $(T_1)_{RKKY}$ is also shown
in Fig.21, where $J\ N(E_F)$ is assumed to be independent of RE species. The
strong RE dependence is observed in $(T_1)_{dipole}$, which is similar to the observed
T_1, while the RE dependence of $(T_1)_{RKKY}$ is weak. If one assumes that
the hyperfine field A_1 arises from 3 neighboring RE moment, $[T_1(Sm)]_{RKKY}$ is 2
times shorter than $[T_1(Sm)]_{dipole}$, while $(T_1)_{dipole}$ is shorter than $(T_1)_{RKKY}$
in other RE based compounds.

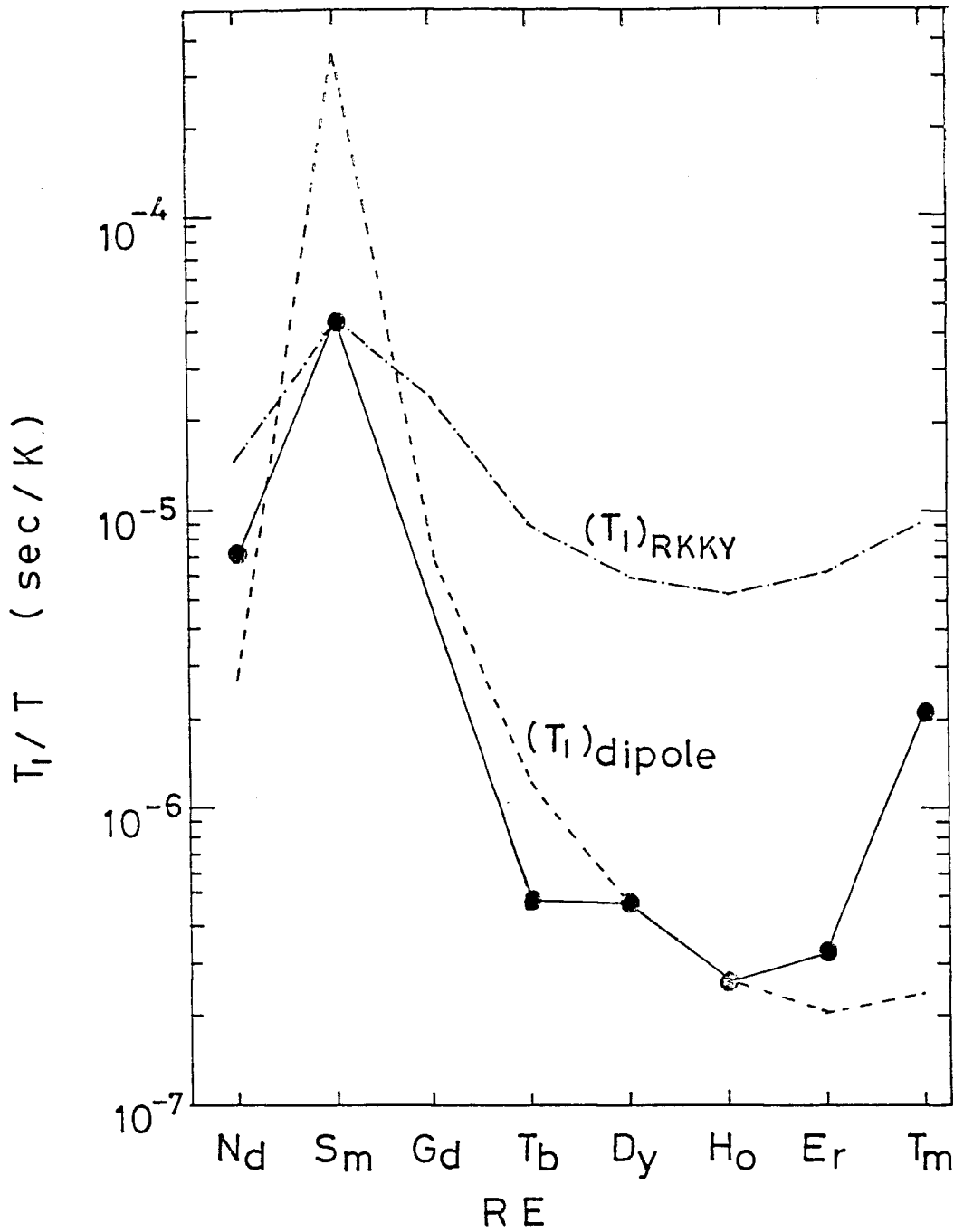Fig.21 The RE dependence of T_1 at high temperature.

(T_1 is determined by Korringa relaxation of the RE spins.)

T_1 due to dipole coupling and RKKY coupling are also shown on the

assumption of $JN(E_F)$ being independent of RE. T_1 due to dipole coupling

is normalized by RE = Dy. T_1 due to RKKY coupling is normalized

by RE = Sm. This value corresponds to the maximum RKKY coupling constant.

So it seems natural to conclude as following.

Even if T_1(Sm) is determined by RKKY interaction, which gives the maximum RKKY coupling constant, T_1 in other RE based compounds is governed by the dipole coupling. Then we obtain $J N(E_F)$ at RE site from the experimental relaxation rate by using eq.28 , eq.29 and $\gamma_e^2 h^2 S(S+1) = \mu_{eff}^2 \times \mu_B^2$. The obtained $J N(E_F)$ is shown in Table 5.

Table 5   Value of $J N(E_F)$ in $RERh_4B_4$

Compound	$J N(E_F)$ [state/atom-spin]
$NdRh_4B_4$	0.16
$TbRh_4B_4$	0.064
$DyRh_4B_4$	0.10
$HoRh_4B_4$	0.10
$ErRh_4B_4$	0.13
$TmRh_4B_4$	0.30

These values obtained in $RERh_4B_4$ are compared with those in Chevrel compounds.[34]

Table 6   Value of $J N(E_F)$ in Chevrel compound

Compound	$J N(E_F)$ [state/atom-spin]
$Eu_{0.25}Sn_{0.75}Mo_6S_8$	0.0033
$GdMo_6S_8$	0.0047
1% Gd in $SnMo_6S_8$	0.0061
0.91% Gd in $SnMo_6S_8$	0.0050

The conduction electron spin polarization in $RERh_4B_4$ is about 20 times larger than that in Chevrel compounds.

(4-3) T_1 of ^{11}B in $RERh_4B_4$ ——— low temperature

Non-S RE ions experiences a relatively large crystal field in $RERh_4B_4$. For example, the Schottky anomalies in specific heat indicate the crystal field effect on RE ions. Recently, Dunlap and Niarchos studied the crystal field effect in $RERh_4B_4$ by analysis of a large amount of available data. Their result is shown in appendix. (In their paper the energy spacing of $|J_z\rangle$ is not published,[31] as it has still ambiguity.)

T_1 is affected by the crystal field effect and is especially sensitive to the ground state at low temperature. For Dy- based rhodium boride the ground state consists of $|\pm 15/2\rangle$ and the first excited state is $|\pm 13/2\rangle$ located by about 130 K above the ground state: $|\Delta m_J| = 1$ transitions are forbidden at low temperature. Then the spin fluctuations associated with the spin-spin interaction (RKKY interaction) and/or s-f exchange interaction are suppressed at low temperature. The spin correlation time τ changes as follows.

1) When τ is determined by RKKY coupling

$$\tau^{-1} \propto \ <\ |<m_f\ |J_\pm|\ m_i>|^2\ >\ \propto\ \exp(-\Delta'/k_R T) \ , \qquad (\ 31\ )$$

2) When τ is determined by Korringa mechanism

$$\tau^{-1} \propto W_\pm \propto |<f\ |J_\pm|\ i>|^2 \cdot \int f(E_i)\cdot[1-f(E_i \mp \Delta')]\cdot dE_i$$

$$\propto \mp \Delta' \cdot \frac{\exp(\mp \Delta'/k_B T)}{\exp(\mp\Delta'/k_B T) - 1}$$

which gives

$$\left\lbrace \begin{array}{ll} W_\pm \propto k_B T & \text{for } \Delta' \ll k_B T \\ \tau^{-1} \propto T & \end{array} \right. ,$$

while

$$\left\lbrace \begin{array}{l} W_+ \propto \exp(-\Delta'/k_B T) \\ W_- \propto \Delta' \qquad\qquad \text{for } \Delta' \gg k_B T \\ \tau^{-1} \propto \exp(-\Delta'/k_B T) \end{array} \right. , \qquad (32\ )$$

Thus

$$T_1 \propto H_{loc}^2 \cdot \frac{\tau}{1 + (\omega_n \tau)^2} \qquad (\ 33\ )$$

$$\propto H_{loc}^2 \cdot \tau \qquad \text{for } \omega_n\tau \ll 1 \quad (\text{ fast limit })$$

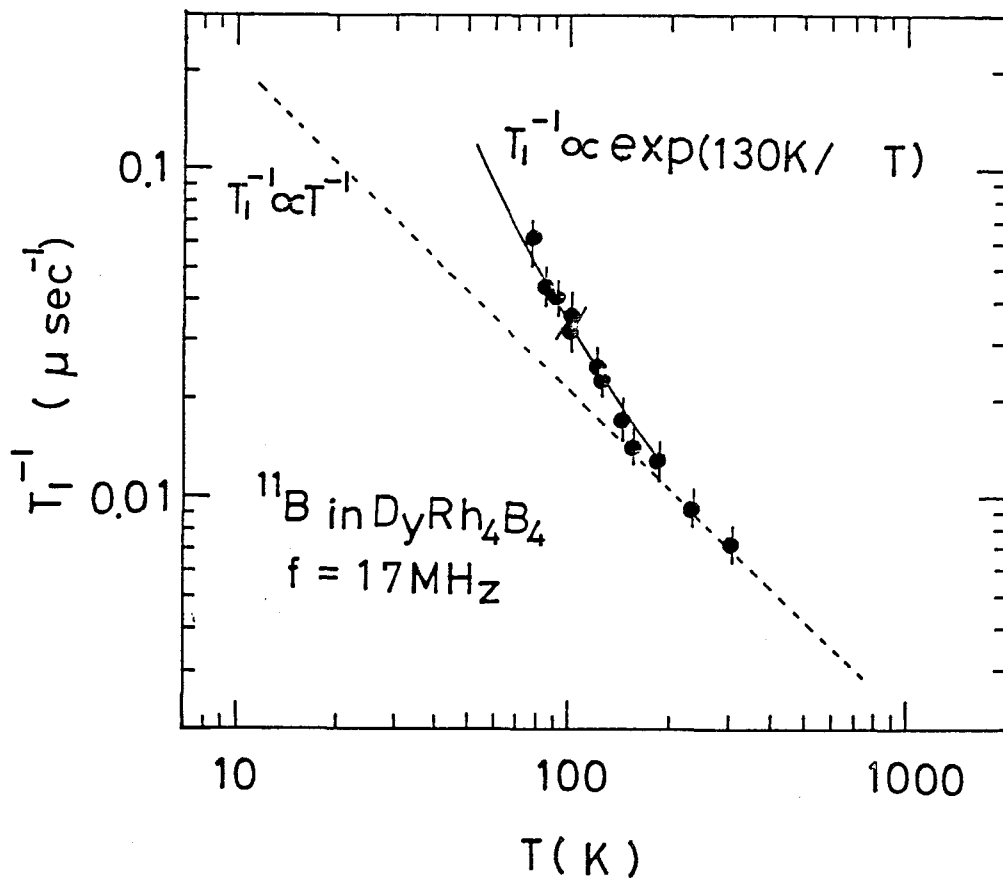while $\propto H_{loc}^2 /(\omega_n^2\ \tau) \qquad \text{for } \omega_n\tau \gg 1 \quad (\text{ slow limit })$

Fig. 22 The temperature dependence of T_1^{-1} of ^{11}B in $DyRh_4B_4$. The system is in fast limit region. The external magnetic field is 12.4 kOe.
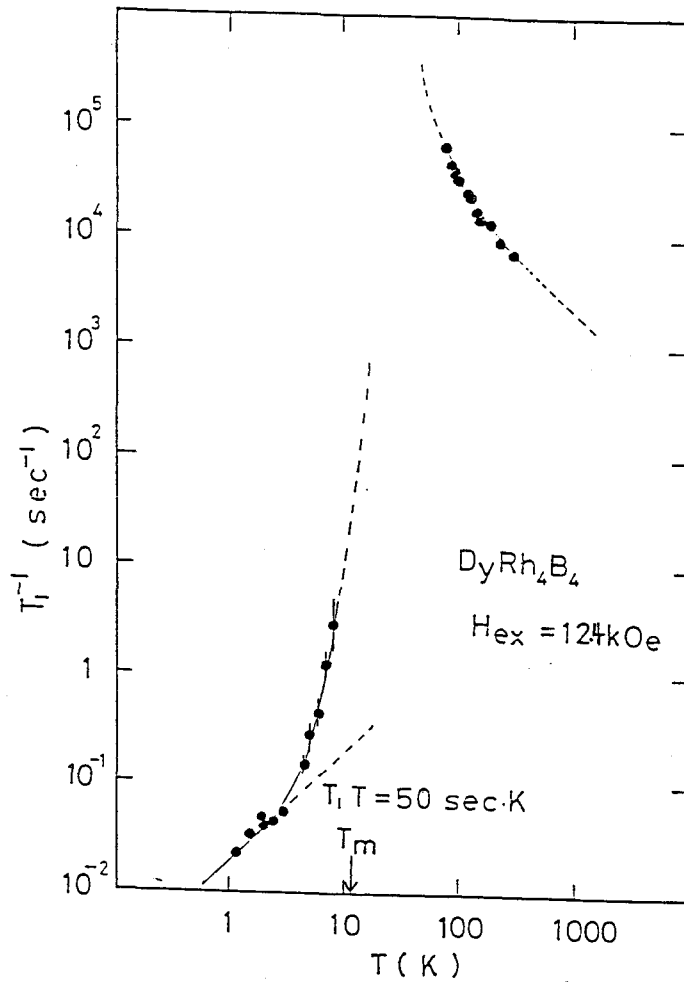

Fig.23 The temperature dependence of T_1^{-1} in $DyRh_4B_4$. At 1.2K T_1 becomes about 10^6 times longer than T_1 at 80K.

Then T_1 of ^{11}B changes exponentially in fast region as shown in Fig.22.

$$T_1 \propto \exp(-\Delta'/k_B T)$$

where Δ' means the energy separation between the ground state$|\pm 15/2\rangle$and

the first excited state$|\pm 13/2\rangle$. The energy gap obtained experimentally is

$\Delta' = 130$K. With further decreasing temperature , τ becomes long and $\omega_n \tau$

becomes larger than 1.(slow limit) Then T_1 increases as τ increases

at low temperature. At 12K the system sets into ferromagnetically ordered

state. Near T_C T_1 increases rapidly with decreasing temperature. Below

4K T_1 is nearly proportional to T^{-1}; $T_1 T = 50$ secK, which is just the same

as in non-magnetic $LuRh_4B_4$. In this temperature region the nuclear spin energy

relaxes to the conduction electron at B site directly and the contribution from

RE spin is negligible. At 1.2K T_1 becomes about 10^6 times longer than T_1 at

80K.

For Sm-based compound the ground state consists of $|\pm 1/2\rangle$, for Er-based

compound the ground state consists of the linear combination of J_z wave functions

of $|\pm 5/2\rangle$ $|\pm 3/2\rangle$ and $|\pm 11/2\rangle$ and for Nd-based compound the ground state is the linear

combination of$|\pm 9/2\rangle$ and $|\pm 1/2\rangle$. These RE based compounds possess

degenerate CFE ground states which are connected by $|\Delta m_J| = 1$ transitions.

The RE spin fluctuation associated with RKKY interaction and/or s-f exchange

interaction is not suppressed in these RE based compounds.

Figure 19 and 24 show the temperature dependence of T_1^{-1}.

T_1 is temperature independent at low temperature (in paramagnetic state) for

Sm and Nd based compound. The spin fluctuation associated with RKKY interaction

is responsible for the temperature dependence, and their behavior is similar

to that in $GdRh_4B_4$.

In $SmRh_4B_4$ T_1 becomes long as the spin fluctuation of the Sm spin is

quenched in magnetically ordered state , as shown in Fig.24. Below 0.3K T_1 is

proportional to T^{-1} ($T_1 T$ = 5 msecK) in the normal state. This value is very

short compared with that in nonmagnetic $LuRh_4B_4$.($T_1 T$ = 55 secK). Therefore ,

the indirect mechanism including the fluctuation of the Sm spin is considered

to contribute to T_1: the indirect coupling between ^{11}B and conduction electron

(virtual excitation of)
through the\ spin waves (Weger mechanism) contributes to T_1 at sufficiently
        32)
low temperature. In this mechanism T_1 is proportional to T^{-1}. As the ground

state is the degenerate$|\pm 1/2\rangle$ the CFE does not yield the energy gap in spin

wave dispersion.in $SmRh_4B_4$. The anisotropy from the dipole coupling of nearest

neighbor Sm is also small as Sm has small magnetic moment. Then the Weger

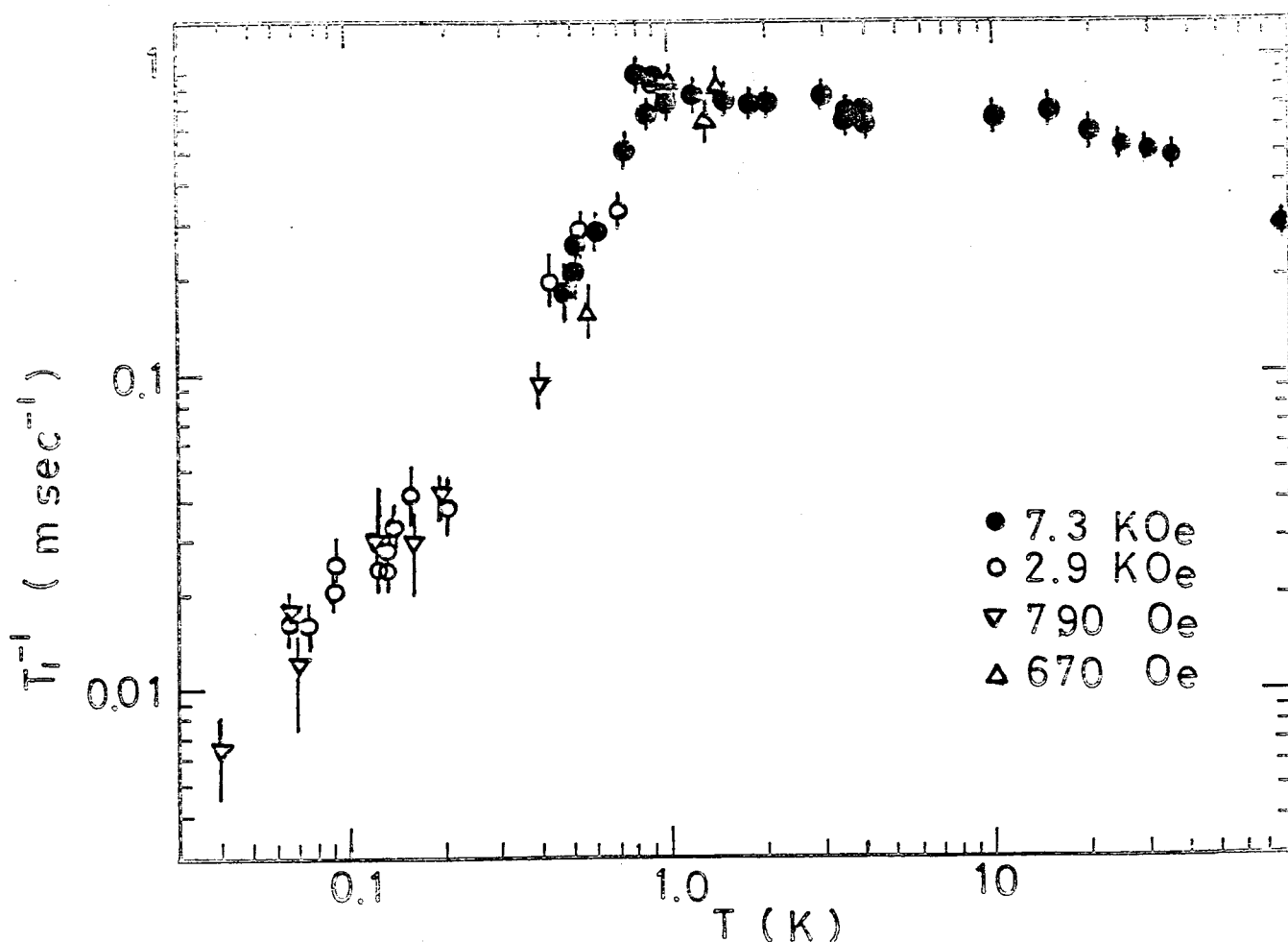mechanism is considered to contribute significantly to T_1.

Fig. 24 Temperature dependence of T_1^{-1} of ^{11}B in $SmRh_4B_4$ below 80K.

(5) Antiferromagnetic superconductor

The coexistence of the superconductivity and the antiferromagnetic order is proposed in $RERh_4B_4$ (RE = Nd, Sm and Tm), $Ho(Ir_{0.7}Rh_{0.3})_4B_4$ and $Dy(Ir_{0.7}Rh_{0.3})_4B_4$. We have obtained NMR spectra of [11]B in magnetically ordered state in $SmRh_4B_4$, $Ho(Ir_{0.7}Rh_{0.3})_4B_4$ and $Dy(Ir_{0.7}Rh_{0.3})_4B_4$.

(5-1) $SmRh_4B_4$

NMR spectra in $SmRh_4B_4$ are shown in Fig.25 and Fig.10-2. Figure25 shows the spectrum in antiferromagnetic and superconducting mixed state.
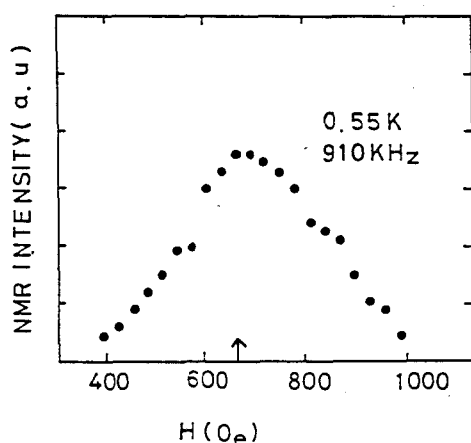

Fig.25 NMR spectrum of [11]B in $SmRh_4B_4$ at T= 0.5 K and f = 910 kHz. The system is in antiferromagnetic and superconducting state.

Figure 10-2 shows the spectrum in antiferromagnetic and normal state. There is no appreciable difference between the line width in superconducting mixed state and normal state. The line width due to the inhomogeneity of the internal field caused by the spatial distribution of vortices is negligibly small compared with the width due to the magnetic origin.

Figure 24 shows the temperature dependence of T_1 in $SmRh_4B_4$. At 790 Oe and 670 Oe the system is in superconducting mixed state. Hence T_1 is expected to increase exponentially in superconducting mixed state, when superconducting energy gap appears in the conduction electron band at Sm site. However, there is

no difference between T_1 in the normal and superconducting mixed state as shown in Fig.24. In the present experimental condition, $SmRh_4B_4$ seems to be gapless superconductor.

Comparing T_s of $LaRh_4B_4$ and $LuRh_4B_4$, [33] we may expect for T_s of $SmRh_4B_4$ to be about 9 K. The actual T_s of $SmRh_4B_4$ is 2.7 K. According to the theory of Abrikosov and Gor'kov on the depression of T_s by the magnetic impurity, the ratio T_s/T_{so} of 0.3 corresponds to a normalized impurity concentration of $n_i/n_{crit} = 0.85$, where n_{crit} is a critical concentration for the occurrence of the superconductivity. In the theory, the depression of T_s by magnetic impurity is accompanied by a change in the excitation spectrum of the superconductor and always leads to a temperature region below T_s where gapless superconductivity occurs. In the case of $T_s/T_{so} = 0.3$ the gap is expected to appear below T/T_{so} = 0.2, T = 1.8 K. Now external field also reduces the energy gap. $SmRh_4B_4$ is considered to be a gapless superconductor above 700 Oe. If we perform the measurement in lower field, we may detect the appearance of the energy gap, although it is difficult to perform NMR study in lower field.

(5-2) $Ho(Ir_{0.7}Rh_{0.3})_4B_4$ and $Dy(Ir_{0.7}Rh_{0.3})_4B_4$

In $Ho(Ir_{0.7}Rh_{0.3})_4B_4$ and in $Dy(Ir_{0.7}Rh_{0.3})_4B_4$ the long range magnetic order and the superconductivity coexist at low temperature. In these compounds the magnetic ordering temperature is higher than the superconducting transition temperature. For Ho-based compound T_M = 2.7 K and T_s = 1.4 K and for Dy-based compound T_M = 4 K and T_s = 1.2 K. The magnetic structure of Ho-based compound is studied by neutron scattering and the result is shown in Fig.28,[30] while the magnetic structure of Dy-based compound is not yet clear.

We observed the zero field NMR in these compounds. Figure 26 and 27 show ^{11}B NMR in Dy-based compound at 1.5 K and Ho-based compound at 0.55 K, respectively.
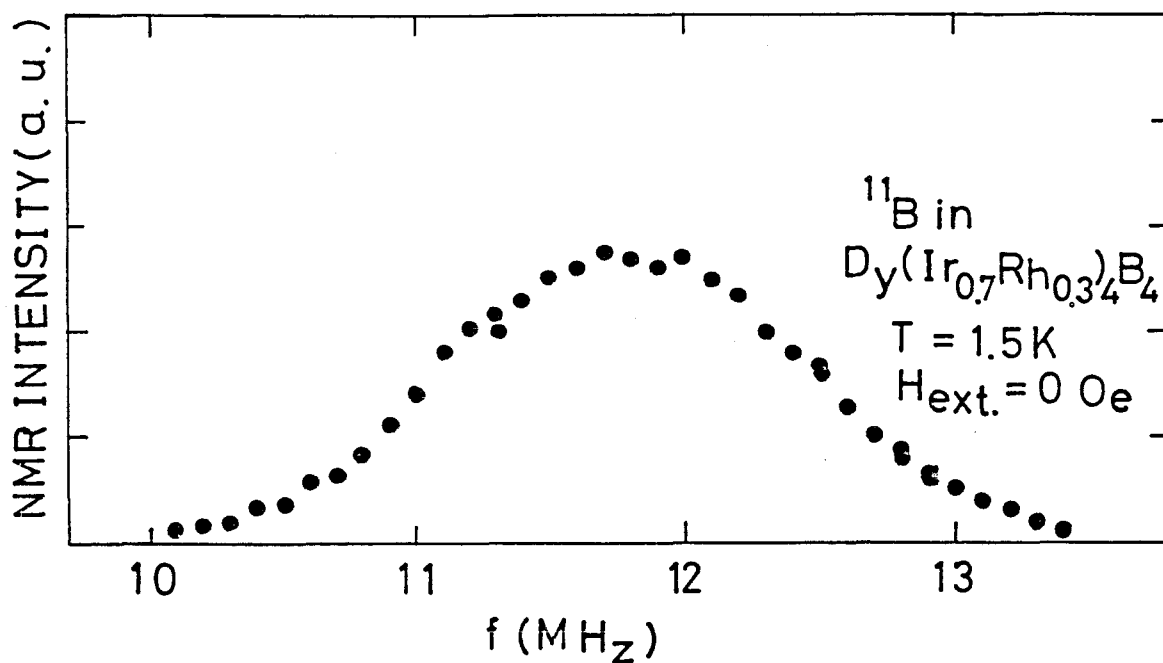
Fig. 26 The zero field NMR spectrum of ^{11}B in $Dy(Ir_{0.7}Rh_{0.3})_4B_4$ at T= 1.5 K.

The system is in antiferromagnetic and normal state.
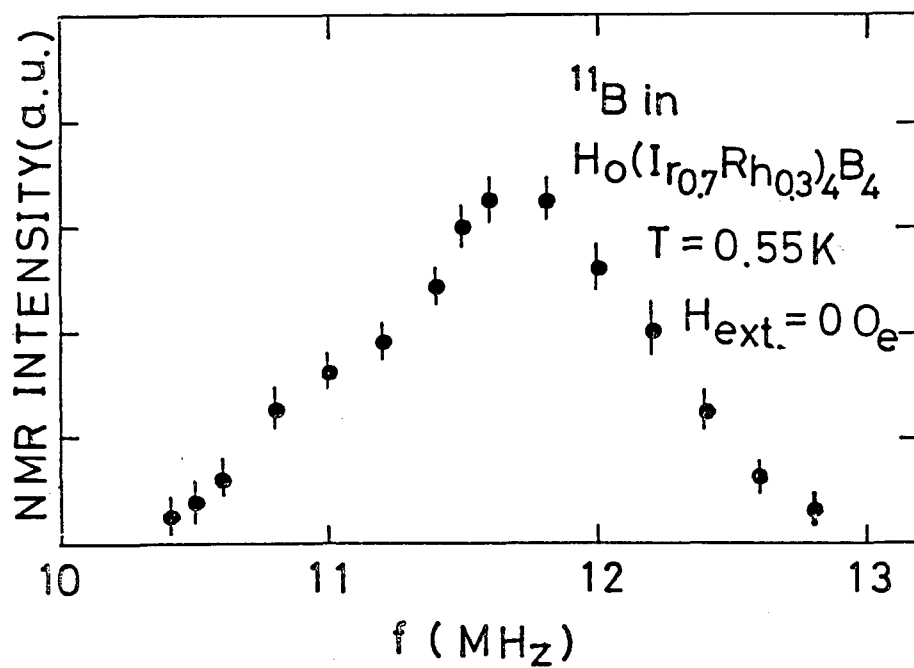
Fig.27   The zero field NMR spectum of ^{11}B in $Ho(Ir_{0.7}Rh_{0.3})_4B_4$ at T = 0.55 K

The system is in antiferromagnetic and superconducting state.

The internal field is 8.6 kOe for the compounds. In the antiferromagnetic compounds the contribution from RKKY coupling becomes small,hence the hyperfine field is determined by the dipole coupling. In Ho-based compound the contribution from the dipole field is 8.6 kOe, which is just the same value as the observed internal field. As the internal field in Dy-based compound is nearly equal to that in Ho-based compound, the magnetic structure in Dy-based compound is considered to be the same as in Ho-based compound.

As T_S and T_M in these compounds are higher than $SmRh_4B_4$, these compounds are good candidate for the study of energy gap ,which is not definite in $SmRh_4B_4$.

$Ho(Rh_{0.3}Ir_{0.7})_4B_4$
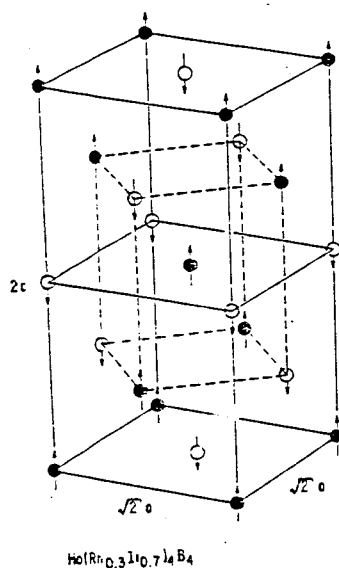
Fig.28 Proposed magnetic structure for $Ho(Ir_{0.7}Rh_{0.3})_4B_4$. The crystallographic unit cell is outlined in dashed lines and the Rh, Ir and B atoms have been removed for clarity.

§5 Conclusion

1) We have measured T_1^{-1} of ^{89}Y (RE site), ^{103}Rh and ^{11}B in YRh_4B_4 and $LuRh_4B_4$ in order to investigate DOS at each atomic site in $RERh_4B_4$. The observed T_1^{-1}'s are compared with the values, which are obtained by using the calculated DOS for $RERh_4B_4$.   The agreement of the experimental results with the band calculation is satisfactory for Y (RE) and Rh site.

Considerable reduction of DOS at RE site(Y site) in $RERh_4B_4$ compared with pure RE metal has been observed, which is responsible for the weak coupling of RE spin and the superconducting electron at Rh site. T_1^{-1} of ^{103}Rh shows a large DOS of d electron at Rh site, which means that Rh is responsible for the superconductivity.

2) We measured the isotropic and anisotropic Knight shift, K_{iso} and K_{anis}, of ^{11}B. K_{iso} of ^{11}B is proportional to the conduction electron spin polarization at B site. We found that it is proportional to $(g_J-1)J$ of each RE. Hence it is concluded that the conduction electron spin polarization induced by unit spin is nearly the same for all $RERh_4B_4$. K_{anis} of ^{11}B is well explained by the   dipole coupling between RE moments and ^{11}B nucleus except in $SmRh_4B_4$. In $SmRh_4B_4$, the anisotropy of the susceptibility seems also to contribute to K_{anis} of ^{11}B.

3) In order to estimate the exchange field on the superconducting electron, we have measured K_{iso} of ^{103}Rh. The isotropic Knight shift arises from s- and d- part of the conduction electron spin polarization. We estimate s-part of the spin polarization at Rh site by assuming that the difference of s-part between B and Rh site is owing to the difference of the hyperfine coupling constant and DOS. Then d- part of the spin polarization is estimated by subtracting s-part from the observed value.

The s-f exchange effect on Rh is one order of magnitude larger than that in Chevrel compound.

4)   The fluctuation of RE moments enhances T_1^{-1} of ^{11}B through the magnetic dipole coupling and the RKKY coupling between RE spin and ^{11}B nucleus. We obtained informations about the origin of RE spin fluctuations, the s-f exchange interaction of RE spin and the conduction electrons at RE site, the indirect coupling of each RE spin through RKKY interaction and also the CFE on the RE spin.

4-1) The s-f and/or d-f exchange interaction at RE site have been obtained from the Korringa spin fluctuation of RE spin. The obtained values are one order of magnitude larger than those found in Chevrel phase compound. This means that s-f exchange interaction play an important role in $RERh_4B_4$ than in Chevrel phase compound.

4-2) Non-S RE ion experiences a relatively large CFE in $RERh_4B_4$, then the energy level of $|J_z>$ is lifted by the CFE. For Dy based compound, the first excited state $|\pm 13/2>$ has been found to be located by 130 K above the ground state $|\pm 15/2>$. This energy spacing is much larger than the exchange interaction between RE ions, then the magnetic properties are much affected by the CFE. This circumstance is also same for all RE in $RERh_4B_4$.

5)   We performed ^{11}B NMR study of non-magnetic superconductor $LuRh_4B_4$ in the superconducting mixed state. $LuRh_4B_4$ is appropriate for the study of superconductivity in the compound without the influence of magnetic interaction or phase transitions. The obtained ratio of the energy gap to the superconducting critical temperature was found to be that of a weak coupling superconductor $2\Delta(o)/k_BT_c = 3.5$.

6) The superconductivity coexists with the antiferromagnetic long range order in $RERh_4B_4$ (RE = Nd, Sm and Tm), $Ho(Ir_{0.7}Rh_{0.3})_4B_4$ and $Dy(Ir_{0.7}Rh_{0.3})_4B_4$. We have obtained NMR spectra of ^{11}B in magnetically ordered state in $SmRh_4B_4$, $Ho(Ir_{0.7}Rh_{0.3})_4B_4$ and $Dy(Ir_{0.7}Rh_{0.3})_4B_4$.

6-1) $SmRh_4B_4$

Below 0.3 K, T_1 is proportional to T^{-1} (T_1T = 5 m sec K) in the normal state. This means that the Weger mechanism governs T_1 at sufficiently low temperature. Thus the nuclear Zeeman energy of ^{11}B relaxes to the conduction electron at RE site. Hence T_1 is expected to increase exponentially in superconducting mixed state, when superconducting energy gap appears in the conduction electron band at Sm site. However, there is no difference between T_1 in the normal state and superconducting mixed state above 790 Oe. $SmRh_4B_4$ is considered to be a gapless or nearly gapless superconductor in the magnetic field of 790 Oe.

6-2) $Ho(Ir_{0.7}Rh_{0.3})_4B_4$ and $Dy(Ir_{0.7}Rh_{0.3})_4B_4$

We have observed the zero field ^{11}B NMR in these compounds. This means the occurrence of the magnetic order in these compounds. For Ho-based compound, the antiferromagnetic order was found by neutron scattering, while the magnetism of Dy-based compound was not clear. From the hyperfine field analysis, we conclude that the magnetic structure in Dy-based compound is the same as in Ho-based compound.

As the superconducting temperature and the magnetic transition temperature in these compounds are higher than $SmRh_4B_4$, these compounds are good candidate for the study of the superconducting energy gap, which is not definite in $SmRh_4B_4$.

Appendix

In $RERh_4B_4$ compounds, the $\overline{4}2m$ point symmetry for the rare-earth ion requires a crystal field Hamiltonian of the form

$$H_{CF} = B_2^0 O_2^0 + B_4^0 O_4^0 + B_4^4 O_4^4 + B_6^0 O_6^0 + B_6^4 O_6^4 \qquad (A-1)$$

where B_n^m's are parameters to be determined empirically and O_n^m's are Stevens operators. Customarily one writes

$$B_n^m = \alpha_n \langle r^n \rangle A_n^m \, , \qquad (A-2)$$

where α_n is a Stevens factor whose value is known but dependent on the individual rare-earth ion under consideration and $\langle r^n \rangle$ is a 4f radial integral obtained from Hartree-Fock atomic calculations. In this form, A_n^m's are determined by the charge distribution in the lattice and are presumed to be approximately independent of the particular rare-earth ion in an isostructural series of compounds. Because of the presence of five unknown parameters in eq.A-1, two of which are multiplied by non-diagonal operators it is difficult to obtain reliable experimental parameters without extensive data and without a priori information on the parameters. Fortunately, in the present case both are available. A Mössbauer measurement of the electric field gradient at the Gd site in $GdRh_4B_4$ has been interpreted to provide a value of A_2^0 which, by use of eq A-2, gives B_2^0 in $RERh_4B_4$. This is an important piece of data since the term in B_2^0 is the largest term in the Hamiltonian.

In addition, single crystal magnetization data has recently been obtained for $ErRh_4B_4$ both parallel and perpendicular to the tetragonal c-axis at various temperatures and fields. In polycrystalline sample, Schottky specific heat datum is available in $ErRh_4B_4$. All the data have been used in non-linear least-square fitting routine to eq.A-1 to obtain the crystal field

parameters, with the B_2^0 value given above as a starting parameter. The results so obtained for $ErRh_4B_4$ are $B_2^0 = 0.769K$, $B_4^0 = 0.13 \times 10^{-2}K$, $B_4^4 = 0.619 \times 10^{-2}K$, $B_6^0 = -0.139 \times 10^{-5}K$, and $B_6^4 = 0.352 \times 10^{-5}K$. The signs of B_4^4 and B_6^4 are indeterminate due to the symmetry of the material. Also using the Er parameter given above in conjunction with eq.A-1 and eq.A-2, wavefunctions and eigenvalues have been computed for a number of rare-earth ions in $RERh_4B_4$ compounds. The results are shown in Table A-1.

Table A-1 Crystal field schemes for (RE)Rh$_4$B$_4$

Nd^{3+} in NdRh$_4$B$_4$

Energy	Level
204.6	$\psi_9\ \psi_{10}$
180.3	$\psi_7\ \psi_8$
158.7	$\psi_5\ \psi_6$
119.6	$\psi_3\ \psi_4$
0	$\psi_1\ \psi_2$

$$\psi_1,\ \psi_2 = 0.997|\mp 9/2\rangle + 0.076|\pm 1/2\rangle$$

$$\psi_3,\ \psi_4 = -0.04|\mp 9/2\rangle + 0.34|\pm 1/2\rangle - 0.94|\pm 7/2\rangle$$

$$\psi_5,\ \psi_6 = 0.68|\mp 5/2\rangle + 0.73|\pm 3/2\rangle$$

$$\psi_7,\ \psi_8 = -0.07|\mp 9/2\rangle + 0.94|\mp 1/2\rangle - 0.34|\pm 7/2\rangle$$

$$\psi_9,\ \psi_{10} = -0.73|\mp 5/2\rangle + 0.68|\pm 3/2\rangle$$

Sm^{3+} in SmRh$_4$B$_4$

Energy	Level
291.9	$\psi_5\ \psi_6$
61.4	$\psi_3\ \psi_4$
0	$\psi_1\ \psi_2$

$$\psi_1,\ \psi_2 = |\pm 1/2\rangle$$

$$\psi_3,\ \psi_4 = |\pm 3/2\rangle + 0.07|\mp 5/2\rangle$$

$$\psi_5,\ \psi_6 = |\pm 5/2\rangle + 0.07|\mp 3/2\rangle$$

Dy^{3+} in DyRh$_4$B$_4$

Energy	Level
373.2	$\psi_{15}\ \psi_{16}$
372.8	$\psi_{13}\ \psi_{14}$
333.2	$\psi_{11}\ \psi_{12}$
316.2	$\psi_9\ \psi_{10}$
281.0	$\psi_7\ \psi_8$
222.9	$\psi_5\ \psi_6$
131.4	$\psi_3\ \psi_4$
0	$\psi_1\ \psi_2$

$$\psi_1,\ \psi_2 = |\pm 15/2\rangle$$

$$\psi_3,\ \psi_4 = |\pm 15/2\rangle$$

$$\psi_5,\ \psi_6 = |\pm 11/2\rangle$$

$$\psi_7,\ \psi_8 = 0.98|\pm 9/2\rangle + 0.20|\pm 1/2\rangle$$

$$\psi_9,\ \psi_{10} = 0.94|\mp 7/2\rangle + 0.30|\pm 1/2\rangle - 0.14|\pm 9/2\rangle$$

$$\psi_{11},\psi_{12} = 0.80|\mp 5/2\rangle + 0.59|\pm 3/2\rangle - 0.06|\pm 11/2\rangle$$

$$\psi_{13},\psi_{14} = 0.93|\pm 1/2\rangle - 0.33|\mp 7/2\rangle - 0.16|\pm 9/2\rangle$$

$$\psi_{15},\psi_{16} = 0.80|\pm 3/2\rangle - 0.59|\mp 5/2\rangle$$

Ho^{3+} in HoRh$_4$B$_4$

$\psi_1 = 0.70|8\rangle + 0.02|-4\rangle + 0.71|-8\rangle$

$\psi_2 = 0.70|-8\rangle - 0.71|8\rangle$

$\psi_3\ \psi_4 = |^+_-7\rangle$

$\psi_5 = 0.70|-6\rangle - 0.70|6\rangle + 0.10|-2\rangle$

$\psi_6 = 0.69|-6\rangle + 0.16|-2\rangle + 0.16|2\rangle + 0.69|6\rangle$

$\psi_7\ \psi_8 = 0.84|\pm5\rangle + 0.48|\pm1\rangle + 0.24|\mp3\rangle$

$\psi_9 = 0.67|0\rangle + 0.53|4\rangle + 0.53|-4\rangle - 0.01|8\rangle - 0.01|-8\rangle$

$\psi_{10} = 0.69|2\rangle + 0.69|-2\rangle - 0.16|6\rangle - 0.16|-6\rangle$

$\psi_{11}\ \psi_{12} = 0.50|\pm1\rangle + 0.71|\mp3\rangle + 0.49|\pm5\rangle$

$\psi_{13} = 0.71|4\rangle - 0.71|-4\rangle$

$\psi_{14} = -0.47|4\rangle - 0.47|-4\rangle + 0.75|0\rangle$

$\psi_{15}\ \psi_{16} = 0.66|\mp3\rangle - 0.72|\pm1\rangle + 0.22|\pm5\rangle$

$\psi_{17} = 0.70|2\rangle - 0.70|-2\rangle$

Er^{3+} in ErRh$_4$B$_4$

$\psi_1\ \psi_2 = 0.69|\mp5/2\rangle - 0.71|\pm3/2\rangle + 0.11|\pm11/2\rangle$

$\psi_3\ \psi_4 = -0.61|\mp7/2\rangle + 0.75|\pm1/2\rangle - 0.24|\pm9/2\rangle$

$\psi_5\ \psi_6 = 0.71|\mp7/2\rangle + 0.39|\mp1/2\rangle - 0.59|\pm9/2\rangle$

$\psi_7\ \psi_8 = 0.71|\mp5/2\rangle + 0.67|\pm3/2\rangle - 0.20|\pm11/2\rangle$

$\psi_9\ \psi_{10} = 0.35|\mp7/2\rangle + 0.54|\pm1/2\rangle + 0.77|\pm9/2\rangle$

$\psi_{11}\ \psi_{12} = 0.22|\pm3/2\rangle + 0.97|\pm11/2\rangle$

$\psi_{13}\ \psi_{14} = |^+_-13/2\rangle$

$\psi_{15}\ \psi_{16} = |^+_-15/2\rangle$

Tm^{3+} in TmRh$_4$B$_4$

330.3 ======== ψ_{12} ψ_{13}

186.1 ======== ψ_{10} ψ_{11}

103.2 ———— ψ_9

99.0 ———— ψ_8

55.3 ======== ψ_6 ψ_7

40.0 ———— ψ_5

3.2 ———— ψ_4

1.3 ======== ψ_2 ψ_3

0 ———— ψ_1

$$\psi_1 = 0.98|0\rangle - 0.14|4\rangle - 0.14|-4\rangle$$

$$\psi_2\ \psi_3 = 0.94|\pm 1\rangle - 0.34|\mp 3\rangle$$

$$\psi_4 = -0.71|2\rangle + 0.71|-2\rangle$$

$$\psi_5 = 0.71|2\rangle + 0.71|-2\rangle$$

$$\psi_6\ \psi_7 = 0.94|\mp 3\rangle + 0.34|\pm 1\rangle$$

$$\psi_8 = -0.71|4\rangle + 0.71|-4\rangle$$

$$\psi_9 = 0.70|4\rangle + 0.70|-4\rangle$$

$$\psi_{10}\ \psi_{11} = |\pm 5\rangle$$

$$\psi_{12}\ \psi_{13} = |\pm 6\rangle$$

Acknowledgements

- 62 -

I would like to express my sincere thanks to Professor K. Asayama for
his valuable discussions and kind encouragements . I would also like to
express my sincere thanks to Professor K. Kumagai for his valuable discussions
Thanks are also due to Drs. T.Kohara, M. Matsumura, Y. Kitaoka
for their discussions.

References

1) M. B. Maple and Ø. Fischer : Superconductivity in Ternary Compounds II
(Springer-Verlag, New York, 1982) chap.2.

2) M. B. Maple and Ø. Fischer : Superconductivity in Ternary Compounds II
(Springer-Verlag, New York, 1982) chap.4.

3) M. B. Maple and Ø. Fischer : Superconductivity in Ternary Compounds II
(Springer-Verlag, New York, 1982) chap.5.

4) M. B. Maple and Ø. Fischer : Superconductivity in Ternary Compounds II
(Springer-Verlag, New York, 1982) chap.8.

5) L.D. Woolf, S. E. Lambert, M. B. Maple, F. Acker, H. C. Ku, W. Odoni
and H. R. Ott, J. Low Tem.Phys. 51 (1983) 117.

6) H. C. Ku and F. Acker, Solid State Comm., 35 (1980) 937.

7) H. C. Hamaker, H. C. Ku, M. B. Maple and H. A. Mook, Solid State Comm.,
43 (1982) 455.

8) T. Jarlborg, A. J. Freeman and T. J. Watson-Yang, Phys. Rev. Lett.
39 (1977) 1032.

9) D. R. Noakes and G. K. Shenoy, Phys. Lett. 91A, 35 (1982).

10) B. T. Matthias, E. Corenzwit, J. M. Vandenberg and H. E. Barz:
Proc. Natl. Acad. Sci. USA 74 (1977) 1334.

11) A. Shawlow and G. Devlin: Phys Rev. 113 (1959) 120.

12) G. C. Carter, L.H. Benett and D. J. Kahn: Metallic Shifts in NMR, Part 1,
Pergamon Press, Oxford, 1977.

13) K. Kumagai and F. Y. Fradin, Phys. Rev. B27 (1983) 2770.

14) T. Asada and K. Terakura, J. Phys. F: Metal Phys 11 (1981) 1847

15) T. Asada, K. Terakura and T. Jarlborg, J. Phys. F: Metal Phys.12 (1982) 1387

16) G. C. Carter, L. H. Bennett and D. J. Kahan: Metallic Shifts in NMR

17) P. G. de Gennes: Superconductivity of metals and Alloys(W.A. Benjamin,
New York, 1966) p.76.

18) A. G. Redfield, Phys. Rev., 125, 159 (1962)

19) D. C. Johnston and B. D. Silbernagel, Phys.Rev. 21 (1980) 4996.

20) Value of these parameters for rare-earth ions are tabulated by P. Fulde,

Physics and Chemistry of Rare-Earths (Edited by K. A. Gshneider, Jr and 1. Eyring)

    300. North Holland, Amsterdam (1970).

21) A. J. Freeman and R. E. Watson,   Magnetism , edited by G. T. Rado and H. Suhl

    (Academic Press Inc., New york, 1965), Vol. IIA, Chap. IV.

22) G. K. Shenoy, D. R. Noakes and D. G. Hinks, Solid State Commun. 42, 411

    (1982).

23) H. C. Hamaker, L. D. Woolf and H. B. Maple, Solid State Comm., 32 (1979)

    289.

24) J. A. Seitchik, V. Jaccarino and J. H. Wernik, Phys. Rev. 138A (1965) 148

25) T. Kohara, Y. Kohori, K. Kumagai and K. Asayama, Phys. Lett. 96A, 8 (1983)

26) G. K. Shenoy, P. J. Viccaro, D. Niarchos, J. D. Cashion, B. D. Dunlap and

    F. Y. Fradin (North-Holland, Amsterdam, 1981) p.209.

27) G. H. Lander, S. K. Sinha and F. Y. Fradin, J. Appl. Phys. 50 (1979) 1990.

28) T. Moriya, Prog. Theor. Phys. 16 (1956) 23.

29) T. Moriya, Prog. Theor. Phys. 16 (1956) 641.

30) H. Hasegawa, Prog. Theor. Phys. 21 (1959) 483.

31) B. D. Dunlap, D.Niarchos, Solid State Commun.44(1982) 1577.

32) M. Matsumura and K. Asayama, J. Phys. Jpn. 43(1977) 1207.

33) H. B. MacKay, L. D. Woolf, M. B. Maple, D. C. Johnston, J. Low Temp. Phys. 44,

    (1980) 639.

34) M. B. Maple and Ø Fischer : Superconductivity in Ternary Compound II

    (Springer-Verlag, New York, 1982) chap.6, p.211.